Novel Physical and Chemical Strategies for Bone Defect Healing

Marianne Comeau-Gauthier, MD

Department of Experimental Surgery

McGill University, Montreal

April 2019

A thesis submitted to McGill University in partial fulfillment of the requirements of the degree of Master of Science.

ABSTRACT

Limb-injuries related to traffic accidents and multiple trauma result in complex treatment needs with substantial socioeconomic impact (*1*). Long bone fractures are often slow to heal and may require months until consolidation is complete, if at all (*2*). Unfortunately for many reasons fracture healing can fail and results in non-union of bone in 10% of all fractures and in up to 50% of open fractures of the tibia (*3*). Thus, there is a need for a novel therapy that stimulates fracture healing but ideally will reduce the invasiveness of treatment and the risk of complications. Here, two new bone healing strategies from distinct approaches are reported: localized cold therapy (physical) and Wnt pathway modulation (chemical).

The first is a non-invasive and novel physical strategy to augment bone healing based on localized cold therapy. Published epidemiological and experimental studies have reported that frequent cold-water exposure results in ectopic bone formation among aquatic sports amateurs (*4, 5*). *In vitro* studies revealed that although osteoclastogenesis is enhanced upon cold application (*6*), the effect of hypothermia on osteoblasts is conflicting (*7, 8*). Aside from case reports of Surfers' Ear there have been no *in vivo* studies on the effect of hypothermia on bone healing. Therefore, we hypothesize that lowering the temperature at the defect site during the healing course may stimulates bone healing. A murine femoral cortical bone defect model was used and cold was applied daily locally through immersion of the lower limb in an ice bath for 15 minutes which was measured as a temperature of 19°C at the bone level.

The second strategy is based on pharmacological treatment to enhance bone healing. A recent published work has demonstrated that Tideglusib, a selective and irreversible small molecule non-ATP-competitive glycogen synthase kinase 3-β (GSK-3β) inhibitor currently in trial for Alzheimer's patients, can promote tooth growth and repair cavities (*9*). Despite some differences,

they are some similarities between bone and tooth formation, and we hypothesize that this new drug could represent a new avenue to stimulate bone healing.

Method – Manuscript #1: The effect of local hypothermia was assessed *in vivo* in a murine cortical bone defect model. Starting on postoperative day 1, one lower extremity was immerged daily in an ice bath for 15 minutes (temperature at bone level=19°C), whereas the other limb was used as control. Mice were euthanized at postoperative day (POD)-7 (early inflammatory phase) and POD-28 (remodeling phase).

Method – Manuscript #2: The effect of localized GSK-3β inhibition was studied using a biodegradable FDA-approved collagen sponge soaked in GSK-3β inhibitor solution or vehicle only (DMSO) and was implanted in 1 x 2 mm unicortical defects created in femora of 35 adult wild-type male mice. Bone defect repair on control and experimental (GSK-3β inhibitor) groups was assessed after 1 week (n=22), 2 weeks (n=24) and 4 weeks (n=24).

Characterization – Manuscript #1-2: For both adjuvants, bone formation was assessed using micro CT and histological analysis alkaline phosphatase (ALP, osteoblasts), tartrate resistant acid phosphatase (TRAP, osteoclasts), CD34, and vascular endothelial growth factor (VEGF, endothelial vascular cells) or immunohistochemistry to confirm the activation of the Wnt/β-catenin pathway.

Results – Manuscript #1: Lowering the temperature at the defect site during the healing course resulted in a significant increase in bone volume, despite a decrease of the osteoblast activity at 4 weeks. Interestingly, immunohistochemical analysis demonstrated higher expression of VEGF and a greater number of CD34+ stained cells during the inflammatory healing stage (1 week) accompanied with higher expression of TRAP. Interestingly, at 4 weeks this trend was inverted, and the expression of VEGF and CD34+ was decreased compared to the non-treated group.

Results – Manuscript #2: Our results showed that Tideglusib significantly enhanced cortical bone bridging (20.6 ±2.3) when compared with the control (12.7 ±1.9; p=0.001). Activity of GSK-3β was effectively downregulated at day 7 and 14 resulting in a higher accumulation of active β-catenin at day 14 in experimental group (2.5±0.3) compared to the control (1.1±0.2; p=0.03). Furthermore, the onset of ALP activity appears earlier in the experimental group (day 14, 1.79±0.28; p=0.03), a level of activity never reached at any end-point by the control defects. At 4 weeks, we observed a significant drop in ALP in the experimental group (0.47±0.05) compared to the control (1.01±0.19; p=0.02) and a decrease in osteoclasts (experimental=1.32±0.36; control=2.23±0.67; p=0.04).

Conclusion – Manuscript #1: Our results demonstrate that daily local cold therapy for 4 weeks accelerates/enhances bone healing in a murine model of intramembranous bone repair. Further, our study suggests that this increase in osteogenesis is mediated by the upregulation of the VEGF pathway. Further studies exploring the mechanism of action of local cooling on bone healing, as well as the optimal treatment dose, duration, and frequency are warranted based on the results of this pilot study. If proven effective, local cold therapy can be introduced as a novel, cost effective, and non-invasive treatment modality to enhance bone healing in a clinical setting.

Conclusion – Manuscript #2: Local downregulation of GSK-3β by tideglusib during bone defect repair resulted in significant increase in amount of new bone formation. The early upregulation of osteoblast activity is one explanation of bone healing augmentation. This is likely the effect of upregulation of β-catenin following pharmaceutical inhibition of GSK-3β since β-catenin activation is known to positively regulate osteoblasts, once committed to the osteoblast lineage. As a GSK-3β inhibitor, Tideglusib demonstrates a different mechanism of action compared with other GSK-3β antagonists as treatment was started immediately upon injury and did not interfere

with precursor cells recruitment and commitment. This indicates that tideglusib could be used at the fracture site during the initial intraoperative internal fixation without the need for further surgery. This safe and FDA-approved drug could be used in prevention of non-union in patients presenting with high risk for fracture-healing complications.

RÉSUMÉ

Les lésions corporelles et polytrauma causés par les accidents routiers nécessitent des traitements complexes causant un lourd impact socioéconomique (*1*). Les fractures des os longs guérissent lentement et plusieurs mois sont nécessaire avant une consolidation complète (*2*). Cependant, environ 10% des fractures ne guériront jamais sans une intervention thérapeutique. On diagnostique alors une non-union osseuse, et ce chiffre peut s'élever à 50% dépendamment de la localisation et du type de la fracture; l'exemple le plus grave étant une fracture ouverte du tibia (*3*). Les cliniciens ont besoin d'une solution qui permettra de guérir les fractures en état de non-unions, idéalement le traitement devrait être minimalement invasif et ayant un faible risque de complications. Cette thèse concerne deux nouvelles stratégies pour accroître la guérison osseuse.
La première stratégie rapportée dans cette thèse est une modalité biophysique n'ayant jamais été employée auparavant pour améliorer la guérison osseuse. Elle se basse sur la thérapie du froid, délivrée de manière local au site de la fracture de façon non-invasive, telle qu'employée pour soulager la douleur lors d'une entorse à la cheville par exemple. Des études épidémiologiques ont rapporté une forte association entre l'exposition chronique à l'eau froide et la formation d'excroissances osseuses au niveau de l'oreille moyenne chez les amateurs de sports aquatiques, et un lien de cause à effet fut par la suite établie en laboratoire (*4, 5*). Des études *in vitro* ont révélés que, bien que l'ostéoclastogénèse s'intensifie lorsque les cellules croient dans un environnement hypothermique, l'effet de cette hypothermie sur les ostéoblastes rapporte des résultats contradictoires (*7, 8*). Hormis les cas d'excroissances osseuses chez les amateurs de sports aquatiques en milieu nordiques, aucune étude *in vivo* n'a été réalisée sur l'effet de l'hypothermie locale sur la guérison osseuse. Un modèle de défaut osseux sur souris a été utilisé pour étudier l'effet de la thérapie par le froid sur la guérison osseuse. Cette thérapie fut appliquée localement

quotidiennement pour 15 minutes, menant à une température d'environ 19C au niveau des tissus environnants.

La deuxième stratégie pour augmenter la guérison osseuse repose sur un traitement pharmacologique appliqué localement durant la chirurgie. Une récente publication fait état du médicament Tideglusib, un inhibiteur sélectif et irréversible se liant de manière non compétitive sur les sites de de liaisons de l'ATP du glycogène synthase kinase 3-β (GSK-3β) à l'heure actuelle utilisé chez les patients atteint d'Alzheimer (*9*). Ce médicament a démontré une augmentation de la guérison dentaire et ayant un effet bénéfique pour la réparation des caries. Malgré que le tissu osseux et le tissu dentaire possèdent des caractéristiques bien différentes, il reste que ces deux tissus partagent bien des similarités. Ainsi, nous croyons que Tideglusib pourrait aussi s'appliquer au niveau du tissu osseux pour en augmenter la guérison.

Méthode – Manuscrit #1 : L'effet de la thérapie par le froid local a été étudié *in vivo* utilisant un modèle de défaut osseux non-critique et unicortical (1x2mm) au niveau des deux fémurs chez la souris. Dès le premier jour post-opératoire, un des deux membres inférieurs a été immergé quotidiennement dans un bain glacé pour environ 15 minutes (atteignant une température de 19C au niveau de l'os), tandis que l'autre membre inférieur a été considéré comme contrôle. Sept souris ont été euthanasiées après 7 jours (phase inflammatoire) et douze souris après 28 jours de traitements (phase de remodelage osseux).

Méthode – Manuscrit #2 : L'effet de l'inhibiteur de GSK-3β, Tideglusib, a été étudié utilisant le même modèle tel que décrit ci-haut sur 35 souris mâles. Une éponge faite de collagène et approuvée par la FDA a été immergée dans une solution de Tideglusib (groupe expérimental) ou contenant seulement le véhicule (DMSO; groupe contrôle). Cette éponge a été par la suite

implantée dans les fémurs lors de la chirurgie. La réparation des défauts osseux des deux groupes a été évaluée après 1 semaine (n = 22), 2 semaines (n = 24) et 4 semaines (n = 24).

Caractérisation – Manuscrit #1-2 : Pour les deux stratégies proposées, la formation osseuse fut évaluée à l'aide du micro-CT et d'une analyse histologique utilisant l'alcaline phosphatase (ALP, marqueur pour les ostéoblastes) et l'acide phosphatase résistante au tartrate (TRAP, marqueur pour les ostéoclastes). Une étude à l'aide de l'immunohistochimie a été réalisée pour étudier soit le facteur de croissance de l'endothélium vasculaire (VEGF, marqueur de la voie de signalement de l'angiogenèse), le CD34 (marqueur de cellules endothéliales), ou des marqueurs de la voie de signalement Wnt/β-caténine.

Résultats – Manuscrit #1 : L'abaissement de la température au niveau du site du défaut osseux par la thérapie par le froid a entrainé une croissance osseuse significative, malgré la diminution de l'activité des ostéoblastes observée à 28 jours de traitement. Fait intéressant, selon l'analyse immunohistochimique les fémurs ayant reçu le traitement par le froid ont démontré une expression plus élevée du VEGF et un plus grand nombre de cellules colorées par CD34 + au stade de la guérison inflammatoire (1 semaine) accompagnée d'une expression plus élevée de TRAP. De plus, cette tendance fut inversée après 4 semaines de traitement lorsqu'on compare le groupe expérimental et le groupe contrôle.

Résultats – Manuscrit #2 : Nos résultats ont montré que Tideglusib améliorait de manière significative la croissance osseuse corticale (20,6 ± 2,3) par rapport au contrôle (12,7 ± 1,9; p = 0,001). L'activité de la forme active de GSK-3β a été efficacement réduite aux jours 7 et 14, ce qui a entraîné une accumulation plus élevée de la forme active de β-caténine au jour 14 dans le groupe expérimental (2,5 ± 0,3) par rapport au groupe contrôle (1,1 ± 0,2; p = 0,03). Coïncidant avec l'augmentation de la forme active de β-caténine, l'expression de l'ALP à 14 jours s'est montré

significativement plus élevée dans ce même groupe lorsque comparé au groupe contrôle. À 4 semaines, nous avons observé une baisse significative de l'ALP dans le groupe expérimental (0,47 ± 0,05) par rapport au contrôle (1,01 ± 0,19; p = 0,02) accompagné d'une diminution du nombre d'ostéoclastes (expérimental = 1,32 ± 0,36; contrôle = 2,23 ± 0,67 ; p = 0,04).

Conclusion – Manuscrit #1 : Nos résultats démontrent qu'un traitement par le froid local et quotidien pendant 4 semaines accélère et améliore la guérison osseuse tel que démontré auprès d'un modèle de défaut osseux non-critique chez la souris. De plus, notre étude suggère que cette augmentation de l'ostéogenèse serait possiblement médiée par la régulation à la hausse de la voie de l'angiogenèse, démontré par une augmentation précoce de l'expression de VEGF. Des études expérimentales supplémentaires seront nécessaires pour explorer et comprendre le mécanisme d'action sous-jacent en plus de déterminer la dose, la durée et la fréquence optimale du traitement par le froid. Si l'efficacité du traitement par le froid est prouvée, le traitement local par le froid pourrait être facilement introduit en tant que méthode non-invasive, et significativement moins dispendieuse auprès des patients afin d'augmenter la guérison osseuse.

Conclusion – Manuscrit #2 : La régulation à la baisse de la forme active GSK-3β par le tideglusib au cours de la réparation d'un défaut osseux a entraîné une augmentation significative de la quantité de formation de nouvel os après 28 jours. La régulation à la hausse de l'activité ostéoblastique, tel que démontré par l'augmentation de l'ALP, auprès des fémurs expérimentaux est certainement une des explications probables de cette augmentation osseuse. Cette augmentation ostéoblastique pourrait être le résultat de la régulation à la hausse de la forme active β-caténine. L'augmentation de l'expression de β-caténine est quant à elle possiblement le résultat de l'inhibition local de GSK-3β. En effet, il a été démontré que β-caténine entraine une augmentation directe du nombre d'ostéoblastes. En tant qu'inhibiteur de GSK-3β, Tideglusib présente un mécanisme d'action

différent de celui des autres antagonistes de la même protéine, car le traitement a été instauré immédiatement après la blessure et n'a pas perturbé le recrutement des cellules précurseurs d'ostéoblastes. Cela indique que tideglusib pourrait être utilisé sur le site de la fracture lors de la fixation interne peropératoire initiale sans nécessiter de nouvelle intervention chirurgicale. Ce médicament sûr et approuvé par la FDA pourrait être une nouvelle modalité d'augmentation osseuse auprès des patients présentant un risque élevé de complications et de non-union.

ACKNOWLEDGEMENTS

I am honored to express my deepest gratitude to my supervisors Dr. Edward Harvey and Dr. Geraldine Merle for their immeasurable support and insightful guidance. Dr. Harvey has shown me the importance of basic research and innovation within surgical orthopaedics. Dr. Merle is an incredible female scientist role model and mentor.

I would like to extend my appreciation to my committee members, Dr. Alice Dragomir, Dr Fackson Mwale and Dr. Bernstein for their teaching and direction. I am also grateful to Dr. Jake Barralet for his scientific guidance.

Special thanks go to Dr. Daniel Castano whom originally had the idea to test cold therapy on bone healing and Dr. Justin Drager for his knowledge on HIF-1α pathway. I want to especially thank Mrs Yu Ling Zhang and Benjamin Dalisson for their technical assistance throughout the process.

I am deeply grateful to Dr. Jose Luis Ramirez-Garcia Luna and Dr. Karla Rangel Berridi from Dr. Henderson's lab for their assistance with surgery, Micro-CT, histology and immunohistochemistry.

This work was supported by grants from the following organizations: Orthopedic Trauma Association, Fonds de Recherche en Santé du Québec and the Research Institute of the McGill University Health Centre.

Finally, to my father, thank you for the love and support

TABLE OF CONTENTS

LIST OF FIGURES AND TABLES

ABBREVIATIONS

6BIO	6-Bromoindirubin-3'-oxime
ALP	Alkaline phosphatase
APC	Adenomatosis polyposis coli
BFR	Bone formation rate
BMPs	Bone morphogenetic proteins
BMD	Bone mineral density
B.Pm	Total bone perimeter
BV	Bone volume
BV/TV	Bone volume/tissue volume
BVV/TV	Blood vessel volume/tissue volume
Cby	Chibby
DA	Degree of anisotropy
DAB	3,3'-diaminobenzidine hydrochloride
Dkk	Dickkopfs
dL. Ar	Double label area
dL.Pm	Double label perimeter
Dsh	Dishevelled
FDF	Fibroblast growth factor
Fzd	Frizzled
GDFs	Growth differentiation factors
GSK-3β	Glycogen syntase kinase- 3beta
H&E	Hematoxylin-Eosin
HIF	Hypoxia-inducible factor
IL	Interleukin
Lef1	Lymphoid enhancing factor 1
LiCl	Lithium chloride
Li_2CO_3	Lithium carbonate
LIPUS	Low-intensity pulsed ultrasonography
LRP5/6	Low-density-lipoprotein-related protein 5 or 6
MicroCT	Microcomputed tomography

MAR	Mineral apposition rate
MMA	Methylmethacrylate
MS/BS	Mineralizing surface/bone surface
MSCs	Mesenchymal stem cells
NHOst	Normal human osteoblasts
PoVop	Open pore volume
ORIF	Open reduction and internal fixation
PBS	Phosphate-buffered saline
PEMF	Pulsed electromagnetic fields
Pocl	Porosity
POD	Postoperative day
RANKL	receptor activator of nuclear factor κB ligand
ROI	Region of interest
Scl	Sclerostin
Sfrp	Secreted frizzled related proteins
sL.Pm	Single label perimeter
TCF	T-cell factor
Tb.N	Trabecular number
Tb.Pf	Trabecular pattern factor
Tb.Sp.	Trabecular separation
Tb.Th	Trabecular thickness
TRAP	Tartrate-resistant acid phosphatase
TGF	Transforming growth factor
TNF	Tumour necrosis factor
TRP	Transient receptor potential
TRPM8	Transient receptor potential cation channel subfamily M member 8
SMI	Structural model index
VEGF	Vascular endothelial growth factor
Wnt	Wingless
WT	Wild-type

CONTRIBUTION OF AUTHORS

The thesis is presented in a manuscript-based format fulfilling the criteria and guidelines outlined by McGill Graduate and Postdoctoral Studies.

Chapter 1 and 2 present a brief introduction and overview of current strategies for bone healing augmentation.

Chapter 4 and 5 represent my experimental work written in the form of two published papers and adapted for the thesis. I performed most of the experiments, collected and analysed the data. I wrote both papers entirely, Drs. Harvey and Merle developed the protocols, supervised and reviewed the manuscripts. The specific contributions of each co-author for each manuscript are outlined below.

Noninvasive localized cold therapy: a new mode of bone repair

The concept was thought by Dr. Daniel Castano and funded through an Orthopedic Trauma Association Resident Grant. He completed the surgery on 12 animals out of 18. Dr. Jose Ramirez GarciaLuna completed the imaging, data collection and analysis of these 12 animals. Dr. Justin Drager provided his expertise on the hypoxia-inducible factor (HIF).

Accelerating fracture repair by activating Wnt/β-catenin signaling pathway via Tideglusib release

Dr. Jose Ramirez Garcia Luna offered several teaching sessions providing me with sufficient knowledge to complete data collection and analysis by myself. Dr. Magdalena Tarchala originally received the Orthopedic Trauma Association Resident Grant.

CHAPTER 1. INTRODUCTION AND RESEARCH OBJECTIVES

Fractures are common traumatic injuries in human. Despite being able to self-heal when treated appropriately after trauma, an estimated 10-15% of fractures do not heal correctly (*10, 11*). The reported incidence and prevalence of non-union vary significantly with the anatomical region and the type of injury (*12*). Furthermore, patient-dependant risk factors include advanced age, specific medical comorbidities (diabetes, vascular disease, osteoporosis), sex, smoking, alcohol abuse, non-steroidal anti-inflammatory use, steroids, chemotherapy, specific genetic disorders, metabolic disease and nutritional deficiency (*13-16*). Patient-independent risk factors include fracture pattern, location, displacement, severity of soft tissue injury, degree of bone loss, quality of surgical treatment and infection (*10, 17*). Multiple definition of non-union and delayed union can be found in the literature, here non-union is defined as an incomplete radiographic healing at 9-12 months, most often accompanied by pain and functional disability. A delayed union shows a slower progression or no progression after 3 months to healing than expected, and is at risk of non-union (*18*). Non-union can be further characterized as hypertrophic (good vascularisation but presence of mechanical instability), oligotrophic (distance gap between the ends of the fracture segments surpassing the healing capacities, caused by critical bone loss or inadequate reduction), atrophic (compromised blood supply, possibly accompanied by mechanical instability), and septic (infection present at the fracture site). When impaired healing occurs, it not only causes chronic pain and disability for the patient, but it presents a frustrating problem for the surgeon as well as a substantial socioeconomic burden (including direct treatment costs as well as personal and societal costs, such as lost wages, decreased productivity and delays returning to work) (*18*).

Some cases of non-union can be initially treated with external bone stimulators (ultrasonic or pulsed electromagnetic waves), but the vast majority will need a surgical intervention coupled with or without some form of biological augmentation. For more than 30 years, a variety of biological, mechanical, and physical therapeutic modalities have been developed to enhance the healing response and fill bone defects, including pulsed ultrasound therapy, biologic adjuvants such as bone morphogenetic proteins (BMPs), and stem cell therapy (*19*). Although these approaches have been shown to have some impact on fracture healing, they are not always cost effective or uniformly successful. Thus, there is a need for a novel therapy that stimulates fracture healing but ideally will reduce the invasiveness of treatment and the risk of complications.

Fracture Healing

Fracture healing can be divided into two types: 1) Primary (direct; intramembranous) healing by internal remodeling and 2) secondary (indirect; endochondral) healing by callus formation. Within the fracture site, intramembranous and endochondral bone healing can occur simultaneously in different regions of the bone healing microenvironment. Cortical (compact) bone comprises 80% of the adult skeleton and is mostly present in the diaphysis of long bones. The stress-oriented collagen fibres are arranged in groups of five to seven concentric rings forming tubular systems (Haversian systems) looping around a central neurovascular channel. Cancellous (trabecular) bone is mainly in the metaphysis and epiphyses of long bones in which Haversian systems are absents and instead assembled in parallel sheets along the axes of mechanical stress. Trabecular bone is comparatively less dense and strong, yet will heal faster than cortical bone (*20*). These subtypes of bone will heal in different ways, here we focus on cortical long bone healing.

Intramembranous ossification during bone development is an important concept, here only intramembranous bone repair will be discussed. Direct (primary or intramembranous) bone healing occurs only with absolute stability and contact of the fragments. Exclusive intramembranous bone healing is rare and refers to a direct attempt of the cells in cortical bone to bridge the discontinuity by Harversian systems without the formation of a cartilage model (*21*). Within a fracture, intramembranous repair occurs subperiosteally at the proximal and distal edges of the callus, in the most mechanically stable regions (*22*). The intramembranous ossification process starts with rapidly expanding localized population of mesenchymal stem cells (MSCs), which will eventually differentiate into osteoblasts. The osteoblasts first produce a non-organized collagenous matrix that will eventually become organized into compact bone, creating new osteons connecting the disrupted fracture fragments (*23, 24*). There are strong similarities between angiogenesis during endochondral and intramembranous repair, however the latter being less understood. Nevertheless, angiogenesis is certainly a prerequisite for ossification during intramembranous osteogenesis (*25, 26*). Osteoclast invasion allows for bone resorption and the creation of further tunnels which enables the in-growth of blood-vessels (*23, 24*).

Fractured bones of the appendicular skeleton heal by both intramembranous and endochondral repair, endochondral bone formation being the primary mechanism responsible for healing. Indirect (secondary or endochondral) bone healing predominates outside the periosteum in regions that are mechanically less stable (*27*). It is distinct from intramembranous ossification as it requires the formation of a cartilage model. Indirect fracture healing is usually driven by some non-excessive micro-motion and weight-bearing (*28, 29*), which promotes cartilaginous callus

formation (*30*). Endochondral bone healing can be divided into four stages: inflammation, soft callus formation, hard callus formation, remodeling.

1. *Inflammatory response:* Fracture leads to disruption of local vessels inside the bone and in the surrounding soft tissue, as well as damage to the other cells and tissues around the injured bone which initiate the acute inflammatory cascade and fracture healing process (*31*). Local disruption of local vessels leads to accumulation of blood in between and around the fracture, where fibrinogen is converted into fibrin generating the fracture hematoma (*23*). The surrounding soft tissue takes on usual characteristics of acute inflammation, demonstrating vasodilatation, hyperemia, and exudation of plasma and leukocytes (*24, 32*). The acute inflammatory response occurs immediately following the trauma, peaks at 24h, and subside after 7 days. At this point, the bone healing microenvironment is characterized by hypoxia and low pH along with peripheral blood-derived inflammatory cells (*33*), together with proinflammatory and anti-inflammatory cytokines (*31*).

   Prolonged inflammatory response is deleterious to bone healing , however a brief and highly regulated secretion of proinflammatory cytokines (tumour necrosis factor-α [TNF-α] interleukin[IL]-1, IL-6, IL-11, IL-18) following the acute injury is critical for tissue regeneration (*21, 34*). The secretion of receptor activator of nuclear factor κB ligand (RANKL), macrophage colony-stimulating factor 1 and members of the transforming growth factor (TGF)-β superfamily (BMPs, TGF-β, growth differentiation factors [GDFs], etc.) are necessary for activate intracellular signalling pathway ultimately affecting gene expression (*34-36*). Hypoxia derived from local abrupt disruption of vascularization promotes the released of angiogenic factors (angiopoetin-1, vascular endothelial growth factor [VEGF]) (*35*) and results in upregulation of the hypoxia-inducible factor (HIF) which further promote VEGF

expression (*37*), in the intent to re-establish normoxic conditions and nutrient supply to the fracture zone which becomes evident at the end of the inflammatory phase.

2. *Soft callus formation:* At this stage, low oxygen and relative instability impairs osteoblast differentiation, but allows chondrocytes proliferation and differentiation (*24*). MSCs differentiate into chondrocytes, which produce a cartilaginous callus template rich in collagen type II and proteoglycans. The relative instability or micro-movements of the fracture fragments further stimulates chondrocytes, and soft callus formation decreases as the fracture becomes mechanically stable (*30*). Once firm mechanical stability is established, the cartilage undergoes hypertrophy and mineralization (*38*). Fourteen days post-fracture, the soft callus will reach its maximal volume. The periosteal reaction, in zones of relative stability, results in early intramembranous ossification.
3. *Hard callus formation:* By day 14, the cartilage from the soft callus begins to calcify (*39*). Chondrocytes mature and become hypertrophic, release calcium and proteases, and undergo apoptosis (*39-41*). Bridging of the fracture fragments with soft callus reduce interfragmentary movement and tissue strain (*42*), allowing blood vessel invasion in the calcified cartilage resulting in hypervascularization of the fracture callus (*43-45*). The newly formed blood vessels enable the recruitment of MSCs, which differentiate into osteoblasts, leading to callus mineralization by deposition of woven bone (in a trabecular structure) in place of the mineralized cartilage (*39*). Cortical bridging of the fracture gap indicates successful fracture healing, which is usually reached after 8-16 weeks in humans (*46*).

   The transition of cartilage to bone via endochondral ossification requires a number of important pathways including Wingless/Integrated (Wnt) signaling pathway, fibroblast growth factor (FGF), Hedgehog, VEGF and HIF (*30, 47, 48*).

4. *Remodeling:* Once the fracture gap is filled by new bone, resorption of the periosteal callus and medullary callus begins with osteoclastic activity at the outer surface. Hypervascularization now subside to pre-fracture levels (*43*). An adequate balance between osteoclastic resorption and osteoblastic formation leads to reshaping of a diaphyseal bone, regenerating the original cortical and trabecular arrangement with a medullary cavity, a process which take years in humans (*43*).

Canonical Wnt signaling pathway

To date, the Wnt signaling pathway have been categorized into two branches: the canonical (Wnt/β-catenin) pathway and the non-canonical (β-catenin-independent) pathway (*49*). Wnts are secreted glycoproteins released in the extra-cellular milieu where they bind to the seven-transmembrane-span protein Frizzled (Fzd) (*50*), an interaction mediated by the low-density-lipoprotein-related protein 5/6 (LRP5/6) (*50*). The signal is then transduced to the cytoplasmic phosphoprotein Dishevelled (Dsh) where it binds to the cytoplasmic tail of Fzd (*51*) and prevents the formation of the β-catenin destruction complex which includes Axin, adenomastosis polyposis coli (APC), glycogen synthase kinase-3β (GSK-3β) and casein kinase 1 (CKK1) (*52*). β-catenin then becomes stabilized and accumulates in the cytoplasm (*52*), and eventually translocates into the nucleus where it interacts with lymphoid enhancing factor-1 (Lef1)/T-cell factor (TCF) DNA-binding transcription factors to exerts its effect on gene transcription (*53, 54*).

Extracellular Wnt pathway antagonists such as Dickkopfs (Dkk) proteins (*55*), Wnt-inhibitor protein (WIF) (*56*), soluble frizzled-related proteins (SFRP) (*57*), Cerebrus (*58*), Frzb (also known as sFRP3, for frizzled motif associated with bone development) (*59*), Sclerostin (Scl) (encoded by the SOST gene) (*60*), Norrin (*61*), and R-Spondin2 (*62*) will prevent Wnt signaling by binding to

Lrp5/6 or by sequestering Wnt proteins (*63*). Fewer Intracellular Wnt antagonists were studied, such as GSK-3β (*64*) Chibby (Cby) (*65*).

The Wnt pathway is intricately involved directly or indirectly in most if not all signal regulation in the heart (*66*), lungs (*67, 68*), liver and kidneys (*69, 70*), gastrointestinal tract (*71*), and bone (*72-74*) and is a major influencer during embryogenesis (*75*), thus it must be targeted safely.

Physical Methods of Bone Healing Augmentation

Mechanical : Mechanical relative stability is a crucial factor for bone healing and is critical element of the diamond concept (*76*). As mentioned above, the progressive maturation of the fracture callus from woven to lamellar bone depends on this stability. According to the Wolff's law, the remodeling of bone is in response to loading and is achieved via mechanotransdution in a process where forces or other mechanical signals are converted to biochemical signals. After an injury, placing specific stress in unique directions facilitates bone remodelling (*77*). Since then, Wolff's law has significantly evolved in clinical setting. Now the open reduction and internal fixation (ORIF) associated to this law is a subtle balance between implant rigidity, relative or absolute fracture stability, fracture gap size, and interfragmentary strain (*78*). The principles of biomechanics are beyond the scope of this work; however, one must keep in mind the importance of relative mechanical stability in bone healing.

Low-intensity pulsed ultrasonography: Low-intensity-pulsed ultrasonography (LIPUS) has been developed around the 1950s and today is primarily applied to the treatment of non-united fracture. In a recent review including 1441 non-unions, LIPUS has shown to have an average healing rate of more than 80% in tibial fracture non-union (*79*), and to be highly successful in treatment of

recalcitrant non-union (*80, 81*). However, more recently, EXOGEN(®), a LIPUS FDA-approved medical device, showed a very low healing of 32.5% in patients with non-union (*82*). Regarding the use of LIPUS on fresh fractures, systematic reviews and meta-analyses on lower and upper extremity fractures confirmed the efficacy of LIPUS treatment on radiographic union, but this was not associated with accelerated functional recovery nor prevention of delayed or non-union (*83-86*). Due to the data discrepancy of LIPUS treatment and its moderate to very low effects on bone healing, LIPUS should be used only on a case-to-case basis.

Pulsed Electromagnetic fields: Pulsed Electromagnetic fields (PEMF) have been studied extensively and are currently used in clinical setting for the treatment of tibial non-unions and long bone delayed unions, with 60% and 80% success rate (*87-97*). There are still some disparities between clinical trials on whether PEMFC enhances bone healing in non-unions and osteotomies despite being approved by the FDA since 2004 (*98-101*). Up to now, current evidence from randomized trials on the effect of PEMF on fracture is its infancy and its benefit of bone growth to reduce the incidence of non-union is inconclusive(*86*).

Thermotherapy: Heat and cold therapies are among the oldest therapeutic modalities to treat orthopedic injuries, and have historically been used as relief for pain (*102-106*), thereby enhancing the rehabilitation process (*107-109*).

1. *Thermotherapy – Heat:* The physiological effects of heat therapy include pain relief, increased blood flow and metabolism which is thought to promote healing by increasing supply of nutrients and oxygen to the site of injury (*110-112*), and increased elasticity of connective tissue which has demonstrated its efficacy for improving range of motion (*113, 114*). The TRP

cation channel subfamily V, members 1, 3 and 4 all respond to warm temperatures (*115, 116*). While heat has been extensively studied for fracture healing, numerous reports have shown inconclusive results on the effect of heat on bone formation (*117-119*). A rat tibial bone defect model subjected local hyperthermia (43C-47C) by magnetic field has shown no difference after 4-6 weeks compared with control (*120*). Similarly, upon local intermittent heat application on a rabbit tibial bone defect model, the bone strength at 3-4 weeks remained unchanged (*121*). More recently, Ota et al (*122*) implanted a heating material in a rat tibial defect model and found after one week treatment that osteogenesis was enhanced. However, the clinical relevance of these non-biodegradable materials needs to be determined as multiple surgeries will lead to inconvenience and morbidity for the patient. An alternative mode of heat therapy is deep-heat therapy, which involves conversion of another form of energy to heat (e.g., shortwave diathermy, microwave diathermy, ultrasound) (*112*). However, their effects on fracture healing have failed to show any significant new bone formation compared to ultrasound and control (*123*).

2. *Thermotherapy – Cold:* Cold therapy is most often used in the management of acute injury, chronic pain, muscle spasm, muscle soreness, and oedema. (*106, 112, 124, 125*). Repeated applications of ice appear to reduce the muscle temperature without compromising the skin, and skin and superficial temperature can return to normal while deeper muscle temperature remains low (*104, 126, 127*). Decreasing the skin and muscle temperature relieves pain, and reduces inflammation, and blood flow to the muscle and bone by activating the sympathetic vasoconstrictive reflex (*128-132*). This results in a slower delivery of inflammatory mediators to the affected area, which attenuates the inflammation response to an acute injury (*133-137*), and decreases the metabolic demand of hypoxic tissue (*138-141*). Local cold therapy induces

a local anesthetic effect by decreasing the activation threshold of tissue nociceptors and the conduction velocity of nerve signals conveying pain (*112, 142-144*), thereby resulting in a higher pain threshold. Key receptors responsive to environmental cold include transient receptor potential (TRP) cation channels subfamily M, member 8 (TRPM8) (*116*).

Cold has significant impact on the properties of the skeletal system *in vivo*. While thermoregulatory adaptation is the widely accepted explanation for the temperature-extremity length phenotype (*145, 146*), environmental modulation of tissue temperature has shown to permanently alter and shorten limbs length of animals raised at cold temperature (*146-155*). In a swine model, whole-body hypothermia has shown to acutely increase local inflammatory molecule (IL-6) in the fracture hematoma, but long-term effects on bone healing was not assessed in this study (*156*). Mice kept at 8C showed delayed tail fracture healing compared to mice kept at 33C (*157*). Although these results together propose intriguing relationships between temperature and bone homeostasis, the effects of intermittent short period cold therapy on long bone healing are yet to be explored.

Biological Methods of Bone Healing Augmentation

The accepted gold standard treatment for augmentation of bone healing is based on traditional bone grafts, specifically autografts due to their obvious intrinsic osteogenic properties (contain living cells capable of differentiation into bone), yet are not always feasible or appropriate (*158*). Autografts have shortcomings: limited availability of bone tissue, increased surgical time, more blood loss, and donor site morbidity (*159*). Due to the significant disadvantages of autograft, research activity has been directed towards alternatives. Allograft and xenograft, in several forms, have been considered as suitable alternatives, but present considerable disadvantages (*160-162*).

Therefore, research has been focussed on synthetic materials with osteoconductive (three-dimensional scaffolds supporting in-growth of new vessels, perivascular tissues and osteogenic cell precursors) or osteoinductive (provides biological stimulus to mesenchymal stem cells driving differentiation into osteoprogenitor cells) capabilities (*20*). To date, the most promising biological enhancement strategies are certainly FGF-2 and platelet-derived growth factors (PDGFs), BMPs, the use of parathyroid hormone (PTH) or Wnt proteins. Locally delivered and/or systemic biological enhancement strategies have been extensively reviewed (*163*), therefore a brief introduction of the most promising modalities and related to this thesis will be discussed here.

BMP

BMPs are local osteoinductive compounds that have been extensively studied in animal models (reviewed in (*164*)) and have been entered in several clinical trials (reviewed in (*165*)), especially BMP-2 and BMP-7. Most BMPs, including BMP-7, provides signals helping the final transition of pre-osteoblasts to osteoblasts (*166*). Recombinant human Bone Morphogenetic Protein (rhBMP)-2 and rhBMP7 have received FDA clearance for treatment of open tibia shaft fractures (INFUSE; Medtronic) and recalcitrant long bone nonunions (OP-1; Stryker), respectively. While the use of localized BMPs has shown promising results in a variety of animal models and different types of fractures and bone defect size, the off-label use of BMPs in humans have been associated with deleterious effects such as wound drainage, neuropathy, neoplasia and excessive bone growth (*167-169*). Currently, even though clinical studies are somewhat heterogenous and present multiple bias, BMP-7 has proven to be beneficial in treating tibial shaft nonunions being at least equivalent to autologous bone graft (*170, 171*) and BMP-2 is to be used in fresh open tibia fractures

with enhanced benefits with higher Gustilo-Anderson types (*172, 173*), although intramedullary nail was a high confounding factor in the BESST trial (*174*).

PTH

PTH is a natural hormone secreted by the parathyroid glands involved in bone homeostasis. In fracture healing enhancement, two molecules have been studied; the active-site portion of the molecule (PTH 1-34) known as teriparatide (TDPT) and the full-length molecule (PTH 1-84). Many different animals models demonstrated that different doses of intermittent teriparatide, whether administered before or after the fracture improved bone mineralization in healthy and osteoporotic fractured model (reviewed here (*175*) and (*176*)). Currently the accepted dosage of 20μg/day of TPDT has shown acceleration of fracture healing in several case controls studies (*177-179*) and improved bone remodeling in distal radius fracture and distal tibia fractures (*180*) in 2 prospective studies. Two other randomized controlled trials did not demonstrate improved radiographic signs of fracture healing nor reduced pain following TPTD treatment in femoral neck fractures (*181*) or proximal humeral fractures in osteoporotic women (*182*). TPTD demonstrated accelerated pubic bone fracture healing and functional recovery in osteoporotic elderly women (*179*). The use of PTH for non-union indicates a possible beneficial effect, however clinical evidence derives from case reports (*183-186*). A recent meta-analysis assembling 380 patients has shown no significant effectiveness regarding time to radiographic union, fracture healing rate or reduction in pain (*187*). However, safety of the molecule was not an issue and merits further investigation and high-quality randomized controlled trials will be needed in the near future to confirm the findings.

GSK-3β

Numerous GSK-3β antagonist molecules have been studies to treat long bone fractures and have shown variable success (**Table 1.1**). Local application of lithium carbonate (Li_2CO_3) immediately after induced tibial defect demonstrated accelerated new bone formation observed at 2 weeks post-injury despite lower mineral apposition rate (*188*). Furthermore, LiCl has shown to restored normal fracture healing and strength in Cx-43-deficient mice and increase fracture healing in healthy mice (*189*), to rescue the damaging effects of alcohol exposure (*190*), as well as improving endochondral repair in an osteoporosis model (*191*). One of the most important finding was the link between the time of onset of lithium treatment and the subsequent improvement in fracture healing. Chen et al. (*192*) were the first to describe repressed fracture healing when systemic lithium chloride (LiCl) treatment was started prior to fracture, where histological results revealed undifferentiated mesenchymal-like tissue. The time of onset was further proved to be the most influential parameter in pre-clinical assessments for optimization and verification using a rodent model of fracture healing (*193, 194*). The authors have concluded that the best regimen corresponds to a dose of 20mg/kg given at day 7 of onset for 2 weeks duration, thereby eliminating the need for a high dosage. An ongoing phase II clinical trial (LiFT) using these exact parameters will help confirmed the effects of lithium on fracture healing [ClinicalTrials.gov identifier: NCT02999022]. AZD2858 was orally delivered to a healthy rat model and has shown increase rate of healing through enhanced intramembranous repair at the expense of endochondral bone formation (*195*). 6BIO has demonstrated to increase proliferation and differentiation of osteoblast and human MSCs (*196-198*), and block the osteoinhibitory action of Dkk-1 (*199*), it failed to augment bone defect healing using either loaded polymeric particles targeting the injured bone or free 6BIO injections (dose: 198μm) in unpublished data (*200*). 6BIO used at a dosage of 0.75mg/kg

injected every 3 days was sufficient to elevate β-catenin expression (qualitative assessment) and rescued the bone healing impairment caused by lead exposure 2 weeks post-fracture (but not at 1 or 3 weeks) (*201*) whereas same or lower dose dosage failed to show enhanced bone healing in normal rodents (*200-202*). Using a different controlled-release system (described below), successful 6BIO micellar delivery has shown increased BV/TV at 3 weeks in a rat femoral fracture model (*202*). While surgically placed drugs have clinical indications, non-invasive systemic delivery can be used as needed for poorly healing bone injuries (*203, 204*). Recent reports using two different GSK-3β molecules (AZD2858, 6BIO) have successfully shown preferential delivery to the fractured bone and biocompatibility in off-target tissues (*205-207*) and subsequent augmentation of fracture healing (*202, 206*).

RESEARCH OBJECTIVES:

1. Physical method of bone augmentation: To confirm that local cold therapy (ice bath of 4-6 °C) can positively affect bone formation in a murine femoral cortical bone defect model.
2. Biological method of bone augmentation: To demonstrate the effect of Tideglusib, a GSK-3β inhibitor, in the treatment of a bone defect rodent model.

TABLE 1.1. Summary of the GSK-3 inhibitors on bone healing

Species	Models	Treatment	Dose	Healing and strength	Major findings	Ref.
Mice	Femur fracture	AZD2858 controlled release[a]	0.168 mg	↑BV/TV, strength	Nanoparticles from controlled release over 9 days showed greater accumulation in fracture bone and accelerated fracture healing (4wks).	(*206*)
		AZD2858 injection[a]		↔BV/TV	At same dose, free AZD2858 failed to accelerate bone healing.	
	Femur fracture	6BIO controlled release[a]	6.9 nmol/kg	↑BV/TV	Micellar delivery of 6BIO controlled release over 7 days showed accelerated fracture healing compared with free 6BIO and control (3wks).	(*202*)
		6BIO injection[a]		↔BV/TV	At same dose, free 6BIO failed to accelerate bone healing.	
	Femur gap defect	6BIO controlled release[a]	198 μm	↔BV/TV	Polymeric nanoparticles showed greater accumulation in fractured bone but failed to improve bone healing (3wks).	(*200*)
		6BIO injection[a]		↔BV/TV	At same dose, free 6BIO failed to accelerate bone healing.	
	Tibia fracture	6BIO injections[b]	0.75 mg/kg	↔callus volume	Free 6BIO failed to accelerate bone healing (3wks).	(*201*)
	Tibial fracture	LiCl PO[c]	200mg/kg	↑BV/TV	Lithium impaired bone healing when started before fracture and enhanced repair when started 4 days after the injury.	(*192*)
	Tibial fracture	LiCl injections[c]	100mg/kg	↔strength	No effect on bone strength (2wks).	(*190*)
	Femur fracture	LiCl PO[c]	200mg/kg	↑BV/TV, strength	Accelerated bone healing and bone strength (3wks).	(*189*)
Rats	Femur fracture	LiCl	20mg/kg	↑BMD, strength	Maximal healing and strength occurred with a low dose (20mg/kg) dose given for a longer time (2wks) with a 7d of onset (4wks).	(*194*)
	Femur fracture	LiCl	20mg/kg	↑strength	Best regimen corresponds to a low dose of 20mg/kg given at 7d of onset for 2wks duration (4wks).	(*193*)
	Tibial gap defect	Li_2CO_3 (localized)	10 mM	↑strength	Accelerated bone healing (2wks).	(*188*)
	Femur fracture	AZD2858 PO daily	30 μmol/kg	↑BMD, strength	Accelerated healing through intramembranous repair without the formation of cartilage (3wks).	(*195*)

[a] One injection
[b] Three injections over 9 days
[c] Treatment was given daily and started 4 days after fracture

CHAPTER 2: NON-INVASIVE LOCALIZED COLD THERAPY: A NEW MODE OF BONE REPAIR ENHANCEMENT

Publication

Daniel Castano‡, Marianne Comeau-Gauthier‡, Jose Luis Ramirez-Garcia Luna, Justin Drager, Geraldine Merle, Edward J Harvey. (2018) **Non-invasive Localized Cold Therapy: A Mode of Bone Repair Enhancement**. Tissue Engineering part A [October 2018]

Presentations

Comeau-Gauthier, M., Castano D., Ramirez GarciaLuna J., Drager J., Merle G., Edward JE. **Non-invasive Localized Cold Therapy: A Mode of Bone Repair Enhancement**; Annual H. Rocke Robertson Visiting Professorship Trauma Resident's Competition Day; McGill University [Mar 2019]

Comeau-Gauthier, M., Castano D., Ramirez GarciaLuna J., Drager J., Merle G., Barralet J., Edward JE. **Non-invasive Localized Cold Therapy Enhances Angiogenesis in Bone Defect Mode**l; Orthopaedic Trauma Association Annual Meeting; Florida [October 2018]

Castano D., Comeau-Gauthier, M., Ramirez GarciaLuna J., Drager J., Merle G., Barralet J., Edward JE. **Daily Cryotherapy Stimulates Bone Healing in a Murine Model**; Canadian Orthopedic Association CORS/CORA Annual Meeting; BC [June 2018]

Castano D., Comeau-Gauthier, M., Ramirez GarciaLuna J., Drager J., Merle G., Barralet J., Edward JE. **Cold Delivered to Bone Causes Bone Growth**. The 19th European Federation of National Associations of Orthopaedics and Traumatology (EFORT) Congress in Barcelona [June 2018]

Comeau-Gauthier, M., Castano D., Ramirez GarciaLuna J., Drager J., Merle G., Barralet J., Edward JE. **Non-invasive localized cold therapy as a new mode of bone repair enhancement**; Annual Fraser N. Gurd Research Day; McGill University [May 2018]

Castano D., Comeau-Gauthier, M., Ramirez GarciaLuna J., Drager J., Merle G., Barralet J., Edward JE. Daily **Cryotherapy Stimulates Bone Healing in a Murine Model**; Annual McGill Visiting Professor – Orthopaedic Surgery Department; McGill University [May 2018]

Castano D., Comeau-Gauthier, M., Ramirez GarciaLuna J., Drager J., Merle G., Barralet J., Edward JE. **Local Cold Therapy Enhances Angiogenesis and Bone Healing in Mice During Bone Defect Repair**; Trainees Seminar; McGill University [Nov 2017]

Posters

Comeau-Gauthier, M., Castano, D., Ramirez GarciaLuna J., Drager J., Merle G., Barralet J., Edward JE. **Non-invasive Localized Cold Therapy as a New Mode of Bone Repair Enhancement**; American Society for Bone and Mineral Research 2018 Annual Meeting [Sep 2018]

Castano D., Comeau-Gauthier, M., Ramirez GarciaLuna J., Drager J., Merle G., Barralet J., Edward JE**. Local Cold Therapy Enhances Angiogenesis and Bone Healing in A Murine Model of Cortical Repair**; RSBO Journée scientifique annuelle; Faculté de médecine Dentaire Université McGill [Jun 2018]

Castano D., Comeau-Gauthier, M., Ramirez GarciaLuna J., Drager J., Merle G., Barralet J., Edward JE. **Local Cold Therapy Enhances Angiogenesis and Bone Healing in A Murine Model of Cortical Repair**; Injury Repair Recovery Program Research Day; McGill University [Jan 2018]

2.1 Authors

Daniel Castano MDCM[1‡] (First Author)

Marianne Comeau-Gauthier MD[2‡] (First Author)

Jose Luis Ramirez-Garcia Luna MD MSc[2,3]

Justin Drager MD MSc[1]

Geraldine Merle PhD[1] (Corresponding Author)

Edward Harvey MD MSc FRCSC[1]

‡ Equal contributions

[1] Department of Surgery, Division of Orthopedic Surgery, McGill University, Montreal, Canada.

[2] Experimental Surgery, Faculty of Medicine, McGill University. Rue de la Montaigne, Montreal, QC, Canada.

Keywords: cold; bone regeneration; mouse model; angiogenesis; osteoclasts, hypoxia

2.2 Abstract

A new bone healing strategy is reported, which is based on localized cold. A murine bone healing model was used, in which an unicortical defect was surgically created bilaterally within the femurs. After daily immersion in an ice bath for 28 days, a large increase in bone regeneration within a femoral cortical defect compared to the non-treated limb was observed. Bone regeneration mechanism within the defect upon cold was studied at 1 and 4 weeks using micro CT and immunohistochemical analysis and compared to the contralateral limb controls. The advanced stage of healing of the bone structure combined with the increase vascular channel density for the

cold treated group matched with an increased expression of VEGF, and a greater number of CD34+ stained cells in the early phase of repair in the cold group. This indicates an elevation in tissue angiogenesis secondary to VEGF expression in the cold group potentially via a temporary vasoconstriction of the local vasculature leading to a temporary state of relative hypoxia. Local cold therapy may be an unrecognized tool with which to accelerate bone regeneration. The absence of observed systemic or local side effects and enhanced bone healing indicates further study is warranted to develop potential clinical protocols.

Statement of impact

A variety of biological, mechanical, and physical therapeutic modalities of varying complexity, efficacy, cost and safety profile have been developed to enhance the bone healing. There have been sporadic reports of spontaneous bone formation following repeated cold exposure. Here we report for the first time, the anabolic effect of cold exposure on bone healing in vivo resulting in a doubling of bone volume. While the precise mechanism is not fully understood, cold is well-known to stimulate osteoclastogenesis and modulate inflammation. The impact of this finding is considerable for tissue regeneration since cold application is non-invasive, safe and easily implemented.

2.3 Introduction

Both epidemiological and experimental studies have reported a phenomenon that surfers exposed to cold water (19°C and lower) for prolonged periods of time develop external auditory canal exostosis, commonly known as surfer's ear. (*4, 5, 208-213*) A similar condition has also been reported in the paranasal sinuses. (*214-217*) The degree of exostosis showed a significant

correlation with cold-water exposure time. (*218-221*) The histopathology of the temporal cortical bone overgrowths from the ear canal consists of loosely organized trabecular surrounded by circumferential subperiosteal lamellar bone and numerous osteocytes- seemingly demonstrating a reparative process. (*5, 214, 222*)

Intermittent local cold therapy is historically used as rehabilitation adjunct after musculoskeletal injury to relieve pain and reduce inflammation. (*103-105, 107-109, 223, 224*) Reported effects include alteration of the tissue metabolism rate, (*138-141*) local vasoconstriction(*129-131*) with resulting hemorrhage (*108, 225, 226*) and oedema control, (*124, 125*) attenuation of the inflammatory response, (*135-137*) and reduction of nerve conduction velocity (*126, 127*) resulting in a higher pain threshold. (*142-144*) While clearly beneficial for symptomatic relief after injury, little is known about the effects of local hypothermia on the regenerative process of healing skeletal tissue and the above phenomena of "surfers ear" implores the exploration of this question.

Bone tissue has been shown to be resistant to harmful effects of cooling *in vitro* if temperatures above 0 C. Chondrocytes will remain alive up to 6 weeks at 4 degrees C, however freezing will invariably kill them. (*227*) The number of osteoclasts differentiated from mononuclear cell cultures derived from mouse marrow showed a 1.5 to 2-fold increase with cold treatment at 34 C.(*6*) However, the effect of hypothermia on osteoblasts has seen conflicting results in the literature. Patel et al concluded that hypothermia inhibits rat osteoblast differentiation following their results. They showed a reduction of trabecular bone structures containing osteoblasts by 75% when cultured for 14-16 days at 35.5°C and by 95% when dropping to 34°C. (*6*) However, human osteoblast cell lines exposed to short-term (e.g., 1h to 24h of hypothermia out of 14 days in culture) hypothermia exhibited an upregulation of Runx2 and osterix, leading to an increase in osteocalcin expression and alkaline phosphatase activity. (*8*) In vivo study on mice exposed at different

temperatures, demonstrates changes in bony phenotypes with cold temperatures stunting growth. (*228*) The authors propose that environmental temperature may alter limb temperature and perfusion influencing bone growth in the developing skeleton. While these results together propose intriguing relationships between temperature and bone homeostasis, the effects of intermittent short period cold therapy on long bone healing have yet to be explored. The aim of this study is to confirm that an internal bone temperature of 19°C achieved through brief daily locally applied cold by immersion in an ice bath of 4-6°C can positively affect bone formation in a murine femoral cortical bone defect model.

2.4 Experimental Section

Cortical Defect Preparation: A murine cortical bone defect model was used to test our hypothesis. This model has proven to generate a reproducible, mechanically stable defect without the need for fixation. (*229-232*) All animal studies were performed after approval by the McGill Facility Animal Care Committee and were conducted in accordance with the Canada Council on Animal Care and the NIH Guidelines for the Care and Use of Laboratory Animals. Eighteen skeletally mature male C3H *wild-type* mice (Charles River Laboratories, Montreal, QC, Canada) aged to 2-3 months (22-26g) were used. Following general anesthesia with isoflurane, the surgical site was disinfected using a 70% ethanol solution. A 5-mm incision was created to access the anterolateral aspect of the proximal femur using the third trochanter as the proximal landmark. The femur was carefully exposed using blunt dissection and was stripped of its periosteum on its anterolateral surface using the third trochanter as a proximal landmark. A 1-mm high-speed burr (Stryker, Hamilton, ON, Canada) was then used to create a 1 x 2.5mm unicortical rectangular window in the anterolateral aspect of the femoral diaphysis, and the periosteum carefully removed using the

third trochanter as the proximal landmark (**Figure 2.1A**). The defects were then completely flushed with phosphate-buffered saline (PBS) to remove all bone fragments. The wound was then irrigated with normal saline and closed with absorbable sutures in layers. Post operatively the mice received a 5-day course of oral antibiotics (Bactrim, Hoffman-La Roche Inc., Mississauga, ON, Canada), and were allowed full weight bearing on both lower extremities. Pain control was achieved with daily carprofen injections (5 mg/kg) for the first three days after surgery. Mice were assessed for general health status by weight and grooming behaviour, as well as for any signs of fracture or infection.

Implementation of Local Cold Therapy: Both hind limbs of the study animals had a surgically created bone defect as above. One hind limb of every mouse was subjected to daily cold treatments and was designated as the experimental group (n=18). The contralateral hind limb, which did not receive any local cold therapy, was designated as the control group (n=18). Before cold bath treatments, surgical wounds were examined to assess for any skin hypersensitivity or dehiscence. We aimed to decrease the local temperature at the defect to approximately 19°C. The temperature goal of 19°C was chosen to reproduce the temperature of the cold irrigation protocol that Fowler used to show an increase in guinea pig ear canal bony overgrowth. (*4*) To confirm this a temperature sensor was implanted between the femur and extensor mechanism at the defect on two pilot study animals, and its wire connector was tunneled proximally and brought out through the skin on the back of the mouse. The exit site and wires were never placed in the cold bath. The temperature readings confirmed that the local temperature decreased to 19 °C after immersion of the whole limb in a 4-6°C cold bath after 2 minutes. The chosen treatment regimen of 15 minutes once per day, was modeled after the early animal studies of low intensity pulsed ultrasound

(LIPUS), which used a similar regimen. (*233*) Starting on postoperative day 1 and for a total of 7 (n=6) and 28 (n=12) consecutive days, one lower extremity of all 18 mice was submerged in a 4-6°C cold-water bath for a total of 15 minutes after undergoing general anaesthesia (isoflurane/inhalant) (**Figure 2.1B**). Care was taken to maintain core temperature throughout the treatment using a heating pad.

Femur Harvest and Microcomputed Tomography (microCT) Imaging: Mice were euthanized at 7 days or 28 days post-operative (PO) by CO_2 asphyxiation under isoflurane induced anesthesia, followed by cervical dislocation. Femurs were dissected free of soft tissue, fixed overnight with 4% paraformaldehyde, washed in sterile PBS and stored at 4°C prior to conducting the assessment of bone healing. Micro computed tomography (Micro-CT) scans were obtained in a Skyscan 1172 scanner (Bruker, Kontich, Belgium) with an Al 0.5mm filter at a voltage of 50kV and a current of 200μA with a spatial resolution of 5 μm/pixel. 3D reconstructions of specimens were made with the associate software (NRecon v1.6.10.4) and loaded into the CTAn software v.1.16.4.1 for quantitative analysis. Two different regions of interest, centered at the middle of the cortical defect, were selected for bone volume/tissue volume (BV/TV) analysis: ROI A = mineralized tissue occupying the 1.5 mm x 0.9 mm x 0.25 mm window defect, and ROI B = a fixed 1mm diameter circle centered on the medullary canal spanning the entire area of the cortical bone defect- the medullary canal adjacent to the window defect and the mineralized tissue within the window defect. Using Grayscale Index from 55 to 255, the total bone volume (BV) was extrapolated from the region of interest. Usual bone parameters were measure for quantification of bone mass and structure such as percentage of bone volume (BV/TV), trabecular number (Tb.N), bone mineral density (BMD), trabecular pattern factor (Tb.Pf), structural model index (SMI), degree of

anisotropy (DA), trabecular thickness (Tb.Th), trabecular separation (Tb.Sp) and porosity (Pocl). Using a quantification of continuous, connected channel volume as a measure for vascularity developed by Bruker (Bruker micro-CT academy 2016 v5.3), (*37, 230*) blood vessel morphology was assessed at 4 weeks PO. The protocol to calculate the volumetric calculation of the blood vessel network, only includes open pores with a diameter above 50μm. Quantitative data for vascular channels includes blood vessel volume/tissue volume (BVV/TV), blood vessel number (No./mm3), blood vessel thickness (μm), blood vessel spacing (μm) and connective density (μm).

Immunohistological Analysis: After micro-CT analysis, the limbs were decalcified with 10% EDTA, embedded into paraffin and 5µm sections prepared with a LEICA 2255 microtome (Leica Microsystems, Concord, ON, Canada). Hematoxylin-Eosin (H&E) staining was used to assess the morphology of tissue. For histochemical study, samples were stained to identify alkaline phosphatase (ALP) activity in osteogenic cells, tartrate resistant acid phosphatase (TRAP) to identify osteoclasts, CD34 for endothelial vascular cells and vascular endothelial growth factor (VEGF) as a potent angiogenic factor. Immunohistochemistry was performed according to the manufacturer instructions. The sections were incubated overnight with primary antibodies specific for VEGF (ABS82, Millipore, 1:1000) and goat anti-rabbit was used as secondary antibody. Antibody binding was detected using the DAKO antigen retrieval system (DAB kit, K3468, USA). The sections were counterstained with haematoxylin, dehydrated, cleared and mounted.

Microscopic images of the stained samples were captured using a Zeiss Axioskop 40 microscope (Carl Zeiss, Toronto, ON, Canada) or captured with Aperio digital pathology slide scanners from Leica Biosystems. All samples underwent histomorphometric calculation of the percentage of stained cells within defined regions of interest using the software ImageJ v.1.6.0 (NIH, Bethesda,

MD, USA). SPSS version 20 (IBM) was used to compare the means of the parameters measured in the control and experimental groups using a Paired Student T-test. Statistical significance was set at $p<0.05$.

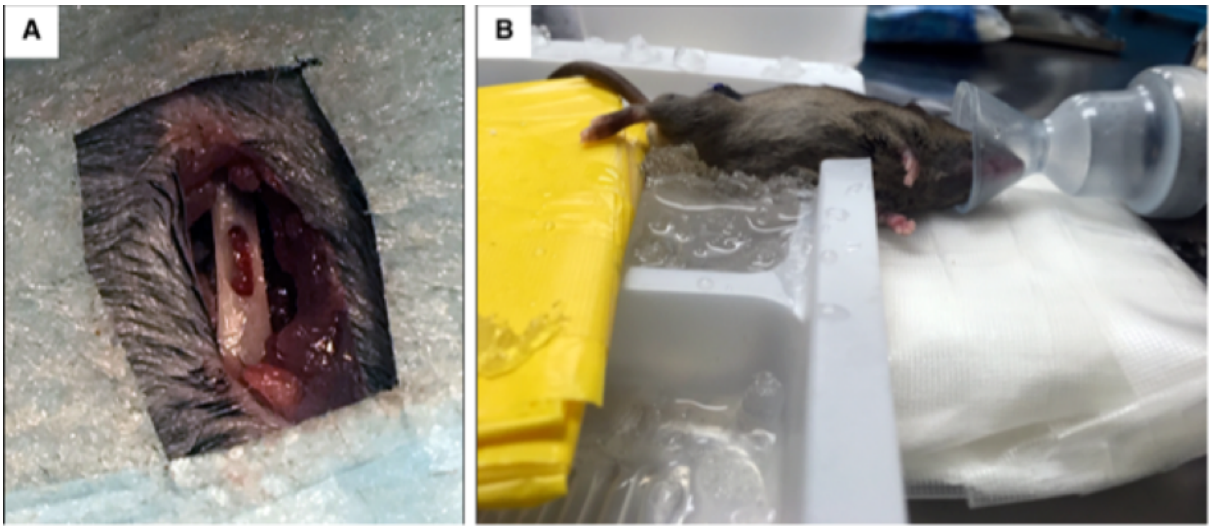

Figure 2.1. Femoral window defect and application of local cold therapy. Bilateral unicortical defects (1mm x 2mm) were drilled into the mid-diaphysis of 2-3 months wild-type C3H mice (**A**). On postoperative day 1, experimental limbs were immerged in a 4-6°C cold bath under general anesthesia for 15 minutes (**B**). Care was taken to completely submerge the hip joint and femur. Contralateral control limbs did not receive local cold bath treatment and were elevated above water level during treatments. Femora were harvested for analysis on postoperative day 7 for 6 mice and on postoperative day 28 for 12 mice.

2.5 Results

A total of 18 mice underwent the operative procedure on both lower extremities without complications. Further, there were no perioperative/postoperative fractures, surgical site infections or signs of deteriorating general health up to the time of euthanasia.

Histomorphometric Analyses

After 1 and 4 weeks, all femora were subject to histomorphometric analysis with micro CT to calculate the amount of new bone formation (**Figure 2.2**). Total bone volume (BV/TV) of each bone was calculated to estimate the bone formation. BV/TV was highest in the cold group at 18.94±9.23 compared to the control limb (7.97±5.13) ($p=0.001$). Bone vessel volume over tissue volume (BVV/TV) was calculated at POD-28 and found to be higher in the cold group compared with control (7.8% vs. 6.7% $p<0.001$) (**Supplemental Figure 2.S1 and Table 2.S1, in Supplementary Information**) and the trabeculae in the defect of cold-treated mice appeared to be thicker, with more dense bone at 4 weeks (**Supplemental Figure 2.S2 and Supplemental Table 2.S2)**.

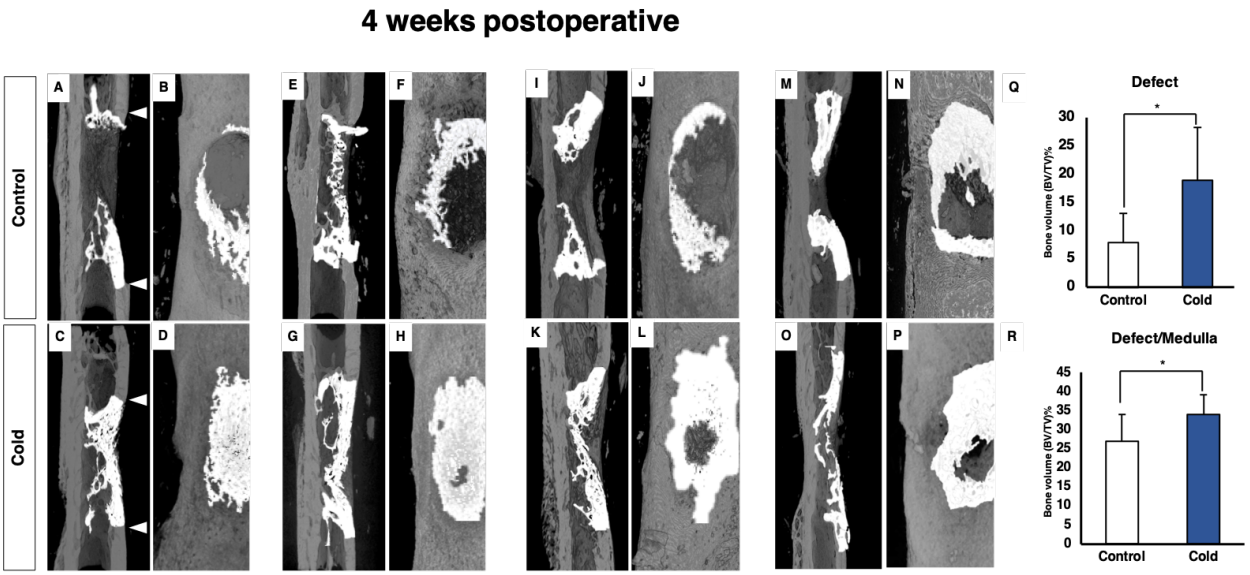

Figure 2.2. **Macroscopic evaluation of bone repair in the window defect**.

Cold-treated and control femora were scanned at a resolution of 5 μm on a Skyscan 1172 instrument. Representative 3D models from paired femora were reconstructed from 2D images to display healing on the defect at 4 weeks postoperative. Significant new bone (white) is seen at the level of the defect in the cold group (C, D, G, H, K, L, O, P) compared to the control group (A, B, E, F, I, J, M, N). The difference in percent bone volume (% BV/TV) in the window defect (ROI A) and in the defect/medullary (ROI B) between the experimental and control group are displayed in the graphs below (Q, R) $p<0.001$. Cold significantly different from control at $p<0.001$.

Histological Observations

Qualitative histological analysis of thin sections of decalcified bone was performed to corroborate the results of the histomorphometric analysis. The staining results for alkaline phosphatase (ALP), tartrate-resistant acid phosphatase (TRAP), presence of vascular endothelial cells (CD34) and vascular endothelial growth factor (VEGF) at both POD-7 and POD-28 are summarized in **Table 2.S2**. ALP staining (**Figure 2.3A-D**) revealed the low number of ALP positive cells at the bone

defect at POD-7 in both non-cold (**Figure 2.3A**) and cold groups (**Figure 2.3B**). After 4 weeks, quantification of ALP stained cells revealed to be significantly decreased ($p<0.001$) in the experimental group (**Figure 2.3D**) compared to the control group (**Figure 2.3C**). Adjacent sections of decalcified bone were stained with TRAP to identify osteoclasts (**Figure 2.3E-H**). A significantly higher number ($p=0.02$) of TRAP positive cells were seen at the proximal ends of the defect at POD-7 in the cold group (**Figure 2.3F**). This suggests an increase in bone turnover at the defect site in the cold-treated femora. At POD-28, an extensive number of TRAP positive stained cells has been detected for the cold group (1.73 ± 0.5) (**Figure 2.3H**), compared to the non-treated bones (1.54 ± 0.4) (**Figure 2.3G**), albeit it did not reach statistical difference. Following H&E staining, fibrous tissue filling the defect area is observed (**Figure 2.4A1, A2**) at POD-7 in both groups. A coarse meshwork of trabecular bone can be seen at POD-28 with bridging of the defect area in the cold-treated limbs (**Figure 2.4A3**), whereas the defect site in control limbs still displayed fibrous stroma with reactive bone formation on the defect edges (**Figure 2.4A4**).

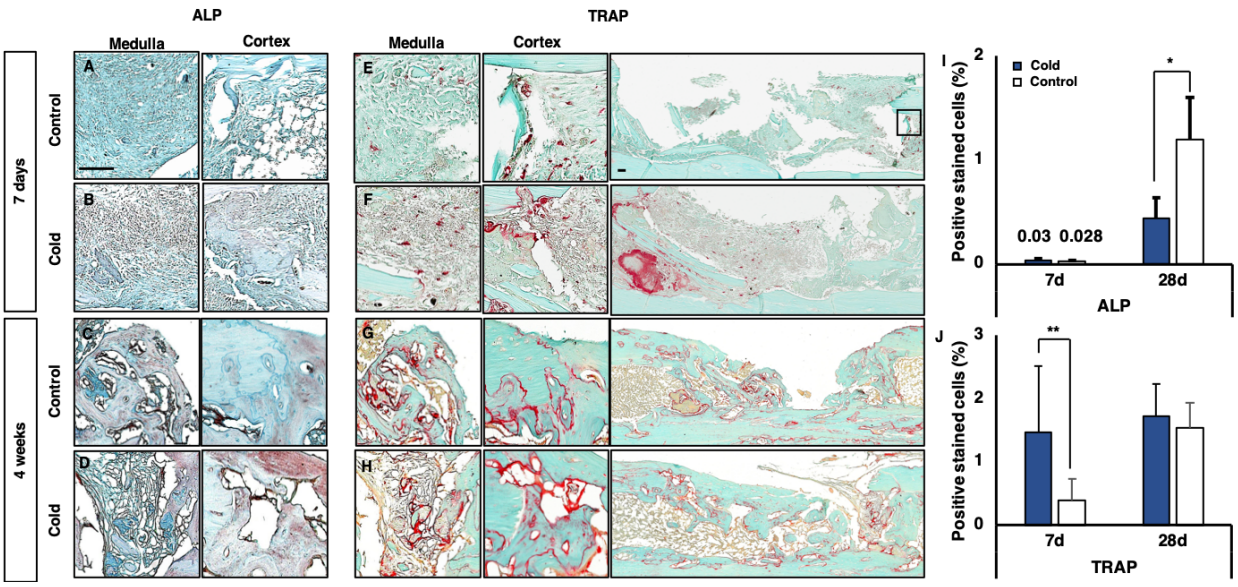

Figure 2.3. Identification of bone-resorbing osteoclasts and bone-forming osteoblasts in regenerating bone. Mid-sagittal sections were harvested from decalcified, paraffin-embedded paired femurs of control and cold therapy at 1 week and 4 weeks postoperative and adjacent sections stained for quantitative analyses of cell composition. Alkaline phosphatase (ALP) staining for osteoblasts showed no difference between control (**A**) and cold treatment (**B**) at POD-7, however osteoblasts were more numerous in the control group (**C**) compared to the cold group (**D**) at POD-28. Tartrate resistant acid phosphatase (TRAP)-positive osteoclasts (red) were less numerous in the control group (**E**) compared to cold treatment (**F**) at POD-7, no difference between the two groups (**G, H**) was seen at POD-28. Right, a graph (**I**) compare the percentage of positively-stained cells between cold and control for ALP and TRAP staining. Images are representative of N = 6 Control and N = 6 Cold at POD-7and N = 12 Control and N = 12 Cold at POD-28. Cold significantly different from control at *$p<0.001$ and **$p=0.03$. Scale bars = 100 µm (A-H).

Immunohistochemical Observations

CD34 was used as a sensitive marker for vascular endothelial cells in soft tissue and bone (**Figure 2.4C1-C4**). The staining showed a significantly higher number of CD34 cells in the cold group (1.03±0.42) (**Figure 2.4C2**) at 7 days compared to the control (0.15±0.09, p = 0.038) (**Figure 2.4C1**). The positively stained-cells were clearly organized into vascular channels. By 4 weeks postoperative, only a few CD34 positive cells persist in the cold-treated femora (p=0.030) (**Figure 2.4C4**), whereas there was a higher expression of CD34 positive stained cells in the control group (**Figure 2.4C3**). VEGF staining was performed to assess the activity of the major angiogenesis pathway (**Figure 2.4D1-D4**). (*234*) A detailed examination of VEGF stained cells in the defect area revealed more pronounced staining at POD-7 in the cold group (15.63±3.51, p = 0.038) than the control group (2.07±0.36) (**Figure 2.4D1**). At POD-28, this trend was inverted, with a VEGF expression significantly higher in the control group (**Figure 2.4D3**) than in the cold group (2.07±0.36 vs. 0.38±0.54, p = 0.034) (**Figure 2.4D4**) and followed the same trend as CD34 staining at POD-28.

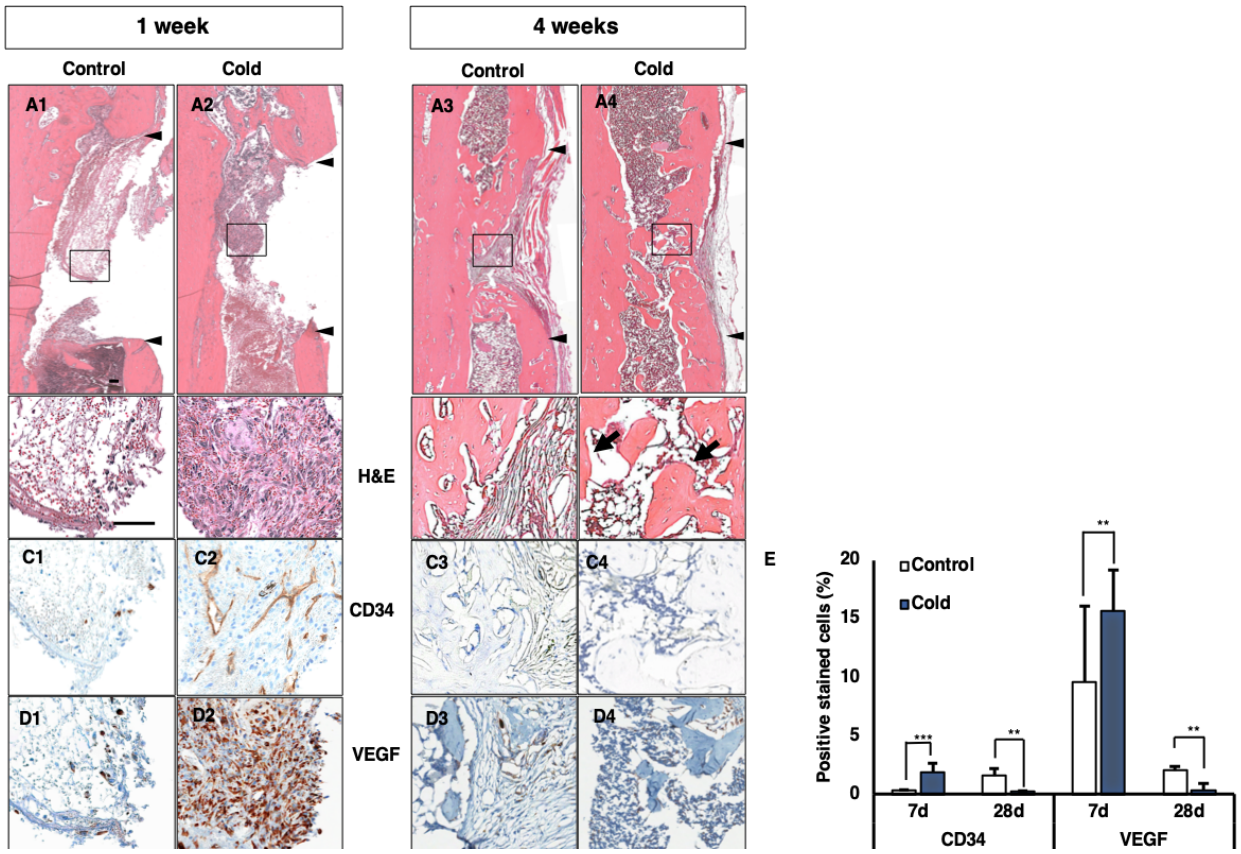

Figure 2.4. CD34 and VEGF immunohistochemistry in regenerating bone. Paired bones were decalcified embedded in paraffin and 5µm sections stained immunochemically for CD34, and VEGF expression for analysis of the inflammatory phase (7 days postoperative) and the remodeling phase (28 days postoperative) of bone healing. Low- magnification images of hematoxylin and eosin-stained sections at 1 and 4 weeks for control (**A1, A3**) and cold (**A2, A4**) groups show the region of tissue (box) where high magnification images were taken (**B1-B4**). At 4-weks postoperative, control defects (**B3**) remained filled with soft tissue whereas cold femurs (**B4**) showed a clear pattern of bone trabeculae surrounded by marrow (arrowheads). Fewer newly formed blood vessels lined with CD34-positive vascular endothelial cells were seen in the non-treated group (**C1**) at 7d PO whereas robust and more pronounced CD34-stained cells organized in vascular channels is seen in the experimental group (**C2**). Representative images of the defect

show less VEGF activity in the control group (**D1**) compared to the cold group (**D2**) at 7 days. CD-34 expression persists at 28d PO in the control group (**C3**) while CD-34 expression becomes near absent in the cold group (**C4**). Whereas at 28d PO, VEGF activity was more pronounced in the control group (**D3**) in comparison with cold group (**D4**). Right, a graph (**E**) compare the percentage of positively-stained cells between cold and control for CD34 and VEGF staining. Images are representative of N = 6 Control and N = 6 Cold at POD-7 and N = 12 Control and N = 12 Cold at POD-28. Cold significantly different from control at **p=0.03 and ***p= 0.04. Scale bars = 500 μm (A1-A4), 50 μm (B1-D4).

2.6 Discussion

This study investigates the effects of a short term localized cold therapy on bone regeneration in an animal long bone defect. Our primary study question showed that a 15 mins of daily immersion in ice cold bath resulted in an increase in bone regeneration within a femoral cortical defect after 28 days of healing time. The similarity in early ALP activity, a marker of osteogenic differentiation, between the cold and control groups supports the hypothesis that the cold induced bone growth might not be mediated by osteoblast activity differences in the early phase of repair. Given that the most probable explanation for the surfer's ear phenomenon may be an increased in osteoblast activity (*211*), here the mechanism of bone healing stimulation following cold therapy might be fundamentally different. Chiba et al has described the distribution of ALP expression in a rat healing model, showing peak expression between days 7-14, after which expression declined as the trabecular bone remodelled. (*235*) Given that the cold limb group at 28 days postoperative exhibited a coarse meshwork of trabecular bone at remodelling phase; this could explain the small amount of ALP expression at that time point. The cold-treated femora might be further along the

remodelling phase when compared to the control group. The advanced stage of healing of the bone structure in the cold group compared with the control was correlated with an increase in estimated vascular channel density at this time point. Both CD34 and VEGF were elevated in the cold therapy group compared to controls at the 7 days indicating an elevation in tissue angiogenesis secondary to VEGF expression in the cold group. VEGF is an essential factor for vascular formation during angiogenesis and vasculogenesis, (*236*) appropriate callus architecture and mineralization in response to bone injury. (*237*) Overexpression of VEGF may induce earlier bone formation and repair when compared to normal level controls. (*238, 239*) Intermittent cold immersion can stimulate the expression of VEGF regulated angiogenic response through hypoxia, endothelial cell stimulation, and direct effect on either bone or blood products. While several studies have shown that short term (*8, 240-242*) and long-term (*6, 243*) hypothermia can have completely opposite effect on bone mineralization, hypoxic stimuli for bone growth has recently been approached by several authors. (*37, 244*) The critical driver in this study may be the intermittent hypoxic microenvironment created during the cold application. Indeed, localized cooling has been shown to cause a decreased blood flow and metabolism in bone(*131*) and significant vasoconstriction continues beyond the cooling period of 20 minutes, despite skin temperatures returning toward baseline values(*130, 135*). Bearing in mind that maintenance of bone oxygen pressure is closely related to the blood flow,(*245*) these results might indicate additive factors affecting the defect model. Cold applied to the bone defect area may cause intermittent hypoxia through vasoconstriction along with the usual disruption of the local blood flow following injury which in turn has been shown to promote osteogenesis, via its upregulation of the angiogenesis pathway (*37, 246*)-whether this is the entire mechanism for cold delivery remains to be seen. In response to a hypoxic environment, Hypoxia-inducible factor (HIF) is activated and

stimulates the transcription of multiple genes with effects on angiogenesis, osteogenesis, precursor cell recruitment and differentiation. (*37, 246*) Finally, osteoclast number was higher in the cold group during the early phase of repair compared to the controls. A stimulatory effect of cold temperature on the formation of human and mouse osteoclasts has been observed *in vitro* where osteoclast number was increased by about 1.5 to 1.7-fold under continuous hypothermic conditions (*6*). However, given the intermittent brief nature of hypothermia in our experiment, the observed elevation in osteoclasts is unlikely to be only explained by a direct effect of temperature change. The elevation of VEGF supports an underlying role of intermittent hypoxia as a potential mechanism for enhancing the bone osteoclastogenesis and the subsequent bone remodelling process. (*247-249*) The positive effects of VEGF activation on osteoclast recruitment and resorptive function have been well documented. (*250, 251*).

Here, we suggest as potential mechanism that localized cold application enhances the bone healing process indirectly, via a temporary vasoconstriction of the local vasculature. This could create a temporary state of relative hypoxia which in turn may lead to upregulation of angiogenic transcription factors (VEGF), thereby improving revascularization and the bone remodelling potential. VEGF and CD34 cells persisted at elevated levels in the control group at 4 weeks, whereas there was a reduction in these markers in the cold-treated group indicating diminishing hemopoietic progenitor cell recruitment at this later time point in the cold group. This is potentially explained by the presence of a more advanced cortical bridging of the defect that is further along the healing sequence in the cold group.

2.7 Acknowledgements

The research was supported by the Orthopedic Trauma Association resident grant.

2.8 Supplementary Information

Supplemental Table 2.S1. Quantitative micro CT analysis of blood vessels.

	28 days postoperative		
	Control	**Cold**	**p value**
	(n=12)	**(n=12)**	
BVV/TV %	6.7 ± 0.9	7.8 ± 0.6	**<0.001**
Blood Vessel Number (No./mm^3)	1.9 ± 0.2	2.0 ± 0.3	0.413
Blood Vessel Thickness (μm)	35.1 ± 2.3	39.5 ± 3.3	**<0.001**
Blood Vessel Spacing (μm)	209.4 ± 22.0	183.8 ± 16.0	**0.010**
Blood vessel Connective Density (μm)	0.37 ± 0.12	0.35 ± 0.12	0.817

BVV/TV = blood vessel volume/tissue volume

Supplemental Table 2.S2. Quantitative analysis of bone architecture at 28 days with micro CT.

	Defect			**Defect/Medulla**		
	Control	**Cold**	**p value**	**Control**	**Cold**	**p value**
	(n=12)	**(n=12)**		**(n=12)**	**(n=12)**	
BV/TV %	7.97±5.13	18.94±9.23	**0.001**	26.9 ± 7.1	34.1 ± 5.0	**<0.001**
Trabecular Number (No./ μm^3)	1.4±0.7	2.80±1.3	**0.003**	3.4 ± 0.7	4.0 ± 0.4	**0.012**
Tb.Th. (μm)	54.6±9.8	67.8±9.2	**0.001**	77.0 ± 7.8	84.7 ± 6.1	**0.001**
Tb.Sp (μm)	213.4±12.9	190.0±25.6	**0.009**	274.5 ± 54.7	235.9 ± 43.8	**0.031**
Connective Density (μm)	0.2±0.1	0.5±0.3	**0.01**	0.53 ± 0.1	0.46 ± 0.1	0.257
Porosity (%)	92.0±5.1	81.1±9.2	**0.001**	73.04 ± 7.1	65.8 ± 5.0	**<0.001**
Number of Closed Pores (No./mm^3)	16.1±15.6	31.8±24.7	**0.05**	274.7 ± 100.0	234.2 ± 136.8	0.451

BV/TV = bone volume/tissue volume; TbTh = trabecular thickness; TbSp. = trabecular separation

Supplemental Table 2.S3. Quantitative staining analysis of cellular activity from paired femora.

	7 days postoperative				28 days postoperative		
	Cold	**Control**	**p value**		**Cold**	**Control**	**p value**
ALP (%) (n=6)	0.031±0.02	0.028±0.01	0.9	ALP (%) (n=12)	0.44±0.2	1.2±0.4	**<0.001**
TRAP (%) (n=6)	1.47±1.08	0.39±0.35	**0.031**	TRAP (%) (n=12)	1.73±0.5	1.54±0.4	0.4
CD34 (%) (n=4)	1.91±0.71	0.31±0.10	**0.046**	CD34 (%) (n=3)	0.22±0.08	1.58±0.6	**0.030**
VEGF (%) (n=6)	15.63±3.51	9.60±6.45	**0.031**	VEGF (%) (n=3)	0.38±0.54	2.07±0.36	**0.034**

ALP osteoblasts; TRAP osteoclasts; CD34 vascular endothelial cells; VEGF vascular endothelial growth factor.

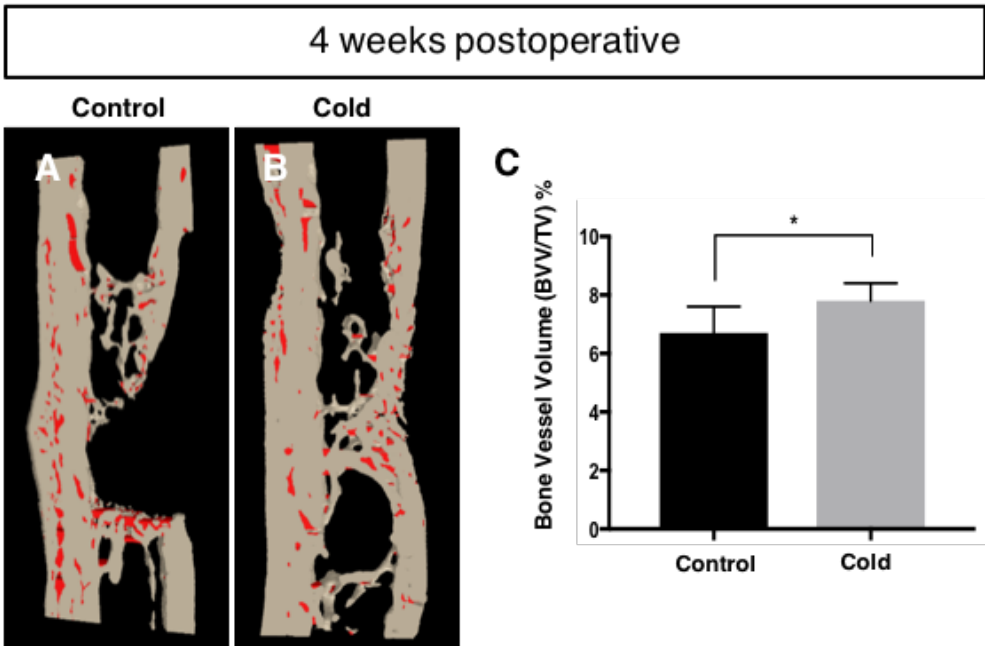

Supplemental Figure 2.S1. Quantitative micro CT evaluation of bone vasculature. Cold-treated and control femora were scanned at a resolution of 5µm on a Skyscan 1172 instrument. *Red* represents connected and uninterrupted channels greater than 50 μm in diameter, which are interpreted as vascular channels. Representative 2D models of paired femora (**A, B**) display the distribution of blood vessels (red) at POD-28. Revascularization is increased in the cold group (**B**). Below, a graph (**C**) compare the percentage of bone vessel volume over tissue volume (BVV/TV)

in the bone between control and cold. Images are from paired femora and representative of N = 12 Control and N = 12 Cold at POD-28. Cold significantly different from control at *p<0.001.

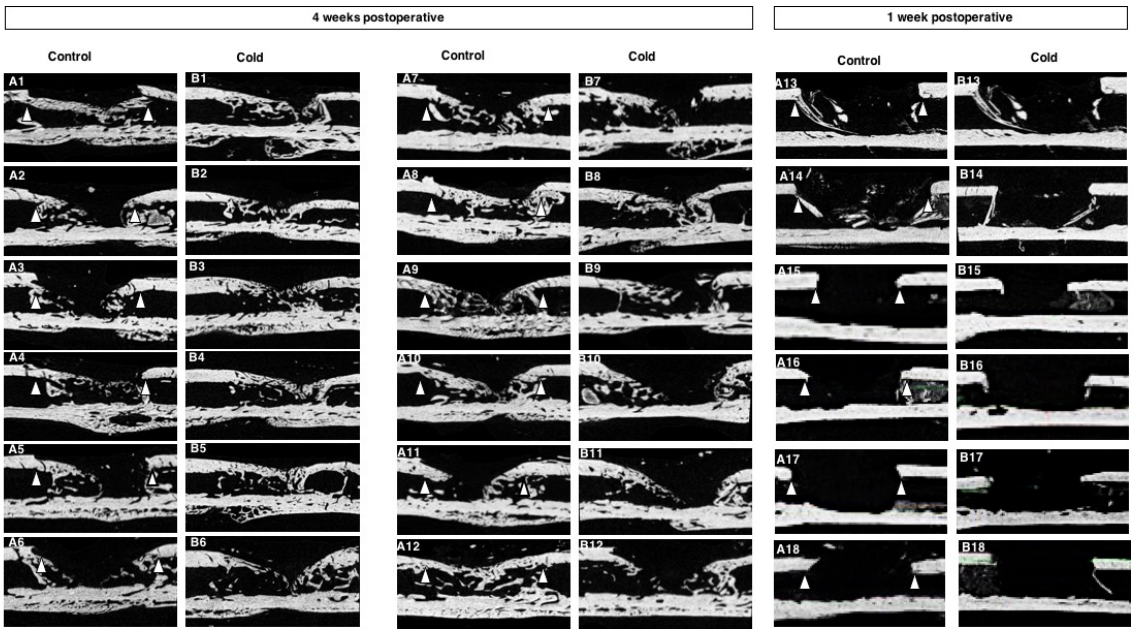

Supplemental Figure 2.S2. Mid-sagittal 2D micro CT images of bone repair. A Skyscan 1172 instrument was used to scan all femora at a resolution of 5 μm. Representative 2D images of paired femora from the control group (A1-A12) and the cold-treated group (B1-B12) are shown after 4 weeks of bone regeneration, and control group (A13-A18) and the cold-treated femora (B13-B18) after 1 week. The arrowheads delineate the proximal (left) and distal (right) margins of the window defect. Bone is seen in the medullary canal and the cortical defect gap. The difference in percent bone volume (% BV/TV) after 4 weeks in the cortical defect gap is statistically higher ($p<0.001$) in the in the cold treated group (18.94±9.23) when compared to the control group (7.97±5.13).

CHAPTER 3. UNLEASHING B-CATENIN WITH A NEW ANTI-ALZHEIMER DRUG FOR BONE TISSUE REGENERATION

Publication

Comeau-Gauthier, M. Tarchala, M. Ramirez GarciaLuna J. Edward JE., Merle G. **Unleashing β-catenin with a new anti-Alzheimer drug for bone tissue regeneration**. Bones [submitted]

Presentations

Comeau-Gauthier, M. Tarchala, M. Ramirez GarciaLuna J. Edward JE., Merle G. **Unleashing β-catenin with a new anti-Alzheimer drug for bone tissue regeneration**; Orthopaedic Trauma Association (OTA) Annual Meeting; Denver US [Sep 2019]

Comeau-Gauthier, M. Tarchala, M. Ramirez GarciaLuna J. Edward JE., Merle G. **Accelerating fracture repair by activating Wnt/β-catenin signaling pathway via Tideglusib release**; International Combined Orthopaedic Research Societies (ICORS)/Canadian Orthopaedic Association (COA) Annual Meeting; Montreal CA [June 2019]

Comeau-Gauthier, M. Tarchala, M. Ramirez GarciaLuna J. Edward JE., Merle G. **Unleashing β-catenin with a new anti-Alzheimer drug for bone tissue regeneration**; Annual Fraser N. Gurd Research Day; McGill University [June 2019]

Comeau-Gauthier, M. Tarchala, M. Ramirez GarciaLuna J. Edward JE., Merle G. **Accelerating fracture repair by activating Wnt/β-catenin signaling pathway via Tideglusib release**; Canadian Connective Tissue Conference (CCTC) Annual Meeting; Montreal CA [May 2019]

Comeau-Gauthier, M. Tarchala, M. Ramirez GarciaLuna J. Edward JE., Merle G. **Accelerating fracture repair by activating Wnt/β-catenin signaling pathway via Tideglusib release**; Annual H. Rocke Robertson Visiting Professorship Trauma Resident's Competition Day; McGill University [Mar 2019]

Comeau-Gauthier, M. Tarchala, M. Ge S. Ramirez GarciaLuna J. Edward JE., Merle G. **Accelerating fracture repair by activating Wnt/β-catenin signaling pathway via Tideglusib release**; Experimental Surgery Graduate Program and Injury, Repair & Recovery Joint Research Day; McGill University [Nov 2018]

Poster

Comeau-Gauthier, M. Tarchala, M. Ge S. Ramirez GarciaLuna J. Edward JE., Merle G. **Accelerating fracture repair by activating Wnt/β-catenin signaling pathway via Tideglusib release**; RSBO Annual Research Day; McGill University [Jun 2019]

3.1 Authors

Marianne Comeau-Gauthier MD[1,2] (First Author)

Magdalena Tarchala MD MSc[1]

Jose Luis Ramirez-Garcia Luna MD MSc[1,2]

Edward Harvey MD MSc FRCSC[1§]

Prof. Geraldine Merle PhD[1§] (Corresponding Author)

[§]*Same contribution*

[1] Department of Surgery, Division of Orthopedic Surgery, McGill University, Montreal, Canada.

[2] Experimental Surgery, Faculty of Medicine, McGill University. Rue de la Montaigne, Montreal, QC, Canada.

Keywords: glycogen synthase kinase 3β; osteoblast; bone regeneration; femur

3.2. Abstract

The Wnt/β-catenin signaling pathway is critical for bone differentiation and regeneration. Tideglusib, a selective FDA approved glycogen synthase kinase-3β (GSK-3β) inhibitor, has been shown to promote dentine formation, but its effect on bone has not been examined. Our objective was to study the effect of localized Tideglusib administration on bone repair. Bone healing between Tideglusib treated and control mice was analysed at 7, 14 and 28 days postoperative (PO) with microCT, dynamic histomorphometry and immunohistology. There was a local downregulation of GSK-3β in Tideglusib animals, resulting in a significant increase in the amount of new bone formation with both enhanced cortical bone bridging and medullary bone deposition. The bone formation in the Tideglusib group was characterized by early osteoblast differentiation

with down-regulation of GSK-3β at day 7 and 14, and higher accumulation of active β-catenin at day 14. Here, for the first time, we show a positive effect of Tideglusib on bone formation through the inactivation of GSK-3β. Furthermore, the findings suggest that Tideglusib does not interfere with precursor cell recruitment and commitment, contrary to other GSK-3β antagonists such as lithium chloride. Taken together, the results indicate that Tideglusib could be used directly at a fracture site during the initial intraoperative internal fixation without the need for further surgery, injection or drug delivery system. This FDA-approved drug may be useful in the future for the prevention of non-union in patients presenting with a high risk for fracture-healing.

3.3 Introduction

Bone regeneration progresses with a well-orchestrated series of biological events of bone induction and conduction, through a number of intracellular and extracellular molecular-signaling pathways. Among them, the Wnt/β-catenin signaling pathway is critical for bone regeneration. Activation of Wnt/β-catenin pathway through the binding of the Wnt protein(*252-255*), downregulates the activity of glycogen synthase kinase (GSK)-3β and leads to hypophosphorylation of β-catenin. The resultant active pathway molecules aggregate and interact with transcription factors that regulate the expression of target genes such as *Axin*, which upregulates osteoblast differentiation (*256*). Because of involvement in several other physiological and pathological processes, such as in the development of tissue fibrosis (*69, 70*), cancer initiation (breast, hepatocellular carcinoma, gliomas) (*257, 258*), and metastasis to bone tissues (*259*), the Wnt/β-catenin signaling must be carefully controlled. Currently, only a few specific biological agents related to the Wnt/β-catenin pathway are in clinical trials or have been used in clinical settings. A recent paper showed that Tideglusib (**Fig. 3.1**), a selective and irreversible small molecule non-

ATP-competitive glycogen synthase kinase 3-β (GSK-3β) inhibitor currently in trial for Alzheimer's disease, promotes tooth re-growth and dental caries repair. (*9*)

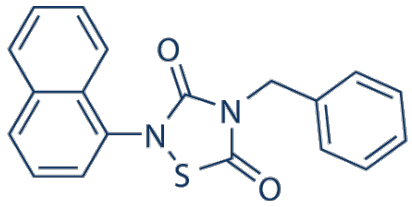

Figure 3.1. Chemical structure of Tideglusib (4-Benzyl-2[naphthlen-1-yl]-1,2,4-thiadiazolidine-3,5-dione), an irreversible, non-ATP-competitive GSK-3β inhibitor.

This study showed that after 6-week exposure to the GSK-3 inhibitor at the injury site, the structure of the dentine was more mature with a similar radiopacity as the surrounding primary/secondary dentine. The expression of Axin 2 was three-fold higher in the presence of Tideglusib than the control group. Dentine is a calcified tissue that has some similarities with bone. Hence, we hypothesized that similarly to the tooth damage, Axin 2 expression and Wnt/β-cat signaling can be upregulated with Tideglusib after bone damage.

Recent data have shown increase gene expression of ß-catenin in all cells located in the fracture callus, suggesting that the Wnt pathway stimulates both intramembranous and endochondral ossification (*255, 260, 261*). The contribution of intramembranous repair to fracture healing has long been observed. Yet, the use of standard fracture models prevents the accurate assessment of its contribution to the bone repair and effectively identify the response of bone marrow-derived cells to endogenous Wnt signalling. In this paper, we report for the first time the effect of Tideglusib in a murine model of bone defect repair that heals through intramembranous

ossification, without an intervening cartilage intermediate, and investigate the underlying mechanism of new bone formation upon GSK-3 antagonist stimulation.

3.4. Material and Methods

Animal model: Animal experiments were performed in strict accordance with the guidelines of the Canada Council on Animal Care. The protocol was approved by the McGill Facility Animal Care committee. Skeletally mature male CH1 wild-type mice aged to 2-3 months (22-26g) were purchased from Charles River Laboratories (Montreal, Quebec, Canada). After 7 days of acclimatization period, a bilateral femoral cortical window defect was surgically created to assess the effect of GSK-3β inhibitor treatment on bone healing as previously described (*262*). Briefly, femora were paired from the same animal; one limb was designated as the experimental group (n=33) whereas the other limb (n=33) was used as control. Following anesthesia with isoflurane, a rectangular window defect measuring 2 mm length x 1 mm depth was fashioned in the anterolateral aspect of the femoral diaphysis using a Stryker drill (Hamilton, ON, Canada). The defect was carefully flushed with phosphate-buffered saline (PBS) to remove any residual bone fragments. Surgifoam sponge (model 12-7, porcine gelatin matrix) supplied by Ethicon Inc. (Somerville, NJ) was used as drug vehicle. Tideglusib (4-Benzyl-2[naphthlen-1-yl]-1,2,4-thiadiazolidine-3,5-dione) was purchased from Sigma-Aldrich (St. Louis, MO). Surgifoam was soaked in DMSO (control) or in DMSO + Tideglusib (50 nM) (*9*). Gelatin sponges were fitted to the window defects and secured with overlying sutured tissues. After surgery, the mice received a 5-day course of oral antibiotics (Bactrim, Hoffman-La Roche Inc., Mississauga, ON, Canada) and were allowed full weight bearing on both lower extremities. Carprofen injections (5 mg/kg) were administered subcutaneously before the surgery and daily for the next three days. Throughout the

duration of the experiment, the animals were left free to roam and with access *ad* libitum to food and water. Mice were assessed for general health status by weight and grooming behavior, as well as for any signs of fracture or infection. The animals were euthanized at 7 days post-operative (PO) (experimental n= 9; control n= 9), 14 days PO (experimental n= 12, control n= 12) and 28 days PO (experimental n= 12; control n= 12) by CO_2 asphyxia under general anesthesia followed by cervical dislocation.

Dynamic Histomorphometry: To study the dynamics of bone defect healing, mice were injected intraperitoneally with 10 mg/kg Calcein in a 2% sodium bicarbonate solution (Sigma-Aldrich) 10 days prior to euthanasia, and 30 mg/kg Alizarin Red in PBS (Sigma-Aldrich) 3 days before euthanasia (*263, 264*). After euthanizing the animals, the femora were harvested, dissected free of soft tissue, fixed for 24h with 4% paraformaldehyde, and washed in sterile PBS and stored at 4°C. Afterwards, the bones were embedded in methylmethacrylate (MMA) following the manufacturer's protocol. Specimens were then cut using a LEICA 2255 microtome (Leica Microsystems, Concord, ON, Canada) to a thickness of 5µm. Axial sections were cut at the mid-point of the defect from three specimens after 4 weeks of bone healing. Images were obtained using a confocal microscope (Zeiss AxioScan Z.1) with a UV light source using red and green filters (465–495 nm). ImageJ v.1.8.0 software (Bethesda, MA) was used to assess the following parameters from areas of new bone formation: total perimeter (B.Pm), single label perimeter (sL.Pm), double label perimeter (dL.Pm), and double label area (dL.Ar). The following values were then calculated: Mineralizing surface/bone surface (MS/BS) = ([1/2sL.Pm + dL.Pm]/B.Pm x 100) (%), Mineral Apposition Rate (MAR)= dL.Ar/ dL.Pm/7 days (µm/day); and Bone Formation Rate (BRF/BS)= MAR x MS/BS x 3.65 ($\mu m^3/\mu m^2$/year) (*189, 265, 266*).

Microcomputed Tomography (microCT) Imaging: Scans of fixed femora were obtained using a Skyscan 1172 instrument (Bruker, Kontich, Belgium) with an Al 0.5 filter at a voltage of 50kV, current of 200μA, and a spatial resolution of 5 μm/pixel, using NRecon v.1.6.10.4 to generate 3D models and CTAn v.1.16.4.1 software for quantitative analysis (Bruker) as described previously (*267*). Two different regions of interest (ROI) were selected for bone volume/tissue volume (BV/TV) analysis: ROI-A (0.9-mm diameter x 1.5-mm) = a cylindrical ROI centered on the medullary canal spanning the entire area of cortical bone defect (Medulla Defect), and ROI-B (1.5 mm x 0.9 mm x 0.25 mm) = mineralized tissue between the proximal and distal ends of the window defect were used for evaluation of bone repair (Window Defect). Usual bone parameters were measured for quantification of bone mass and structure including the percentage of bone volume/tissue volume (BV/TV), trabecular number (Tb.N), trabecular thickness (Tb.Th), trabecular separation (Tb.Sp), porosity (Pocl), open pore volume (PoVop), open porosity, closed porosity, and connective density.

Histology, Histochemistry, and Immunohistochemistry: The harvested limbs were decalcified in a 10 % EDTA solution, embedded in paraffin and cut into 5 microns sections using a LEICA 2255 microtome (Leica Microsystems, Concord, ON, Canada). Serial 5-μm thick sections were cut and stained with hematoxylin and eosin for morphology assessment, and Masson's trichome was used to discriminate collagen fibers. Alkaline phosphatase-positive osteoblasts were observed by staining with Naphthol AS-TR, N,N-dimethyl formamide and NBT/BCIP in 0.25mM tris-maleate buffer (pH 9.3) for 70 minutes at 37°C. Tartrate resistant acid phosphatase (TRAP)-positive cells, used to identify osteoclasts, were observed by staining with Naphthol AS-TR phosphatase, sodium

nitrite, sodium tartrate, and pararosaniline hydrochloride in acetate buffer (pH 5.0) for 40 minutes at 37°C (*232*). Microscopic images of the stained samples were captured using a Zeiss Axioskop 40 microscope (Carl Zeiss, Toronto, ON, Canada). Quantification of histochemical staining was done within defined regions of interest using color deconvolution with Image J software (NIH, Bethesda, MD, USA), as previously described (*268, 269*). Staining intensity is expressed as % of the total area of the ROI and was done in a blinded fashion. Undecalcified specimens embedded in MMA corresponding to 4 weeks of bone healing were stained with Von Kossa to assess mineralized tissue.

For immunohistochemical staining, sections were processed by deparaffinization in Citrisolv (Fisher), dehydration through degraded alcohols. Antigen retrieval for all proteins were done in a 10mM citrate buffer (pH 6.0) solution for 10 minutes at 95°C in a water bath. Endogenous peroxidase activity was blocked using 3% hydrogen peroxide (H_2O_2), and sections were blocked with 5% goat serum for 1 hour at room temperature. The serial sections were incubated in a humidified chamber at 4°C with primary rabbit-anti-mouse antibodies including, GSK3β antibody (1:200, ab32391, total GSK3β), phospho-Tyr216-GSK3β (pGSK3β-Tyr216) 1:50, ab75745, active form), and non-phospho(active) β-catenin (Ser33/37/Thr41) (1:800, CST #8814). The slides were then washed and incubated with SignalStain® Boost IHC Detection Reagent (HRP, Rabbit CST #8114) for 30 minutes at room temperature. Staining was visualized by using 3,3'-diaminobenzidine hydrochloride (DAB) as the substrate chromogen and Gill's Hematoxylin as a counterstain. The confirmed mouse normal gastrointestinal tissues expressing the above proteins were used as positive control, while in the negative control; primary antibody was replaced by isotype specific immunoglobulin G (**Supplementary information, Figure S1**). Quantification of chromogen intensity in the immunohistochemical was performed using Image J software with IHC

Toolbox plugin automated image analysis application. Images were uploaded and analyzed as recommended by the application. Briefly, the DAB quantification option is chosen, and the DAB tissue image is then separated from hematoxylin counterstaining. The image is then converted to a gray scale and a threshold is applied in order to eliminate unspecific staining. The average gray value is then collected. The same threshold is applied to all tissue samples in order to ensure consistency (*270-272*).

Statistical Analysis: Data were expressed as mean ± standard error of the mean. SPSS version 20 (IBM) was used to compare the means of the parameters measured in the control and experimental groups using a Paired Student T-test. Statistical significance was set at $p<0.05$.

3.5 Results

Effect of local GSK-3□ inhibitor release on bone histomorphometry

Bone defect repair in both control (collagen sponge) and experimental (collagen sponge with GSK-3β inhibitor) groups was assessed with microCT after 1-week (n=23), 2 weeks (n=24) and 4 weeks (n=24) PO (**Fig. 3.2A-J**). There were no perioperative/postoperative side effects, infections or signs of deterioration in the animals. A significant increase in bone volume relative to tissue volume (BV/TV) in both regions of interest (ROI-A and ROI-B) was observed after postoperative day (POD-) 28 for the experimental group. Medullary callus (ROI-A) gradually appeared from POD-7 to POD-14 but no difference was demonstrated ($p>0.05$) between the control (POD-7: 0.04 ±0.02; POD-14: 4.76 ±1.22) and experimental (POD-7: 0.35 ±0.25; POD-14: 4.82 ±0.86) groups (**Fig. 3.2M**). However, the medullary bone increased significantly from POD-14 to POD-28, with a much higher bone growth in the GSK-3β inhibitor-treated group (43.31 ±2.67) compared to the

vehicle alone (control) (36.53 ±2.88) after 4 weeks of healing (p=0.014). The difference between control and experimental groups was more pronounced in the cortical defect (ROI-B) area after 28 days (**Fig. 3.2N**) whereas no differences were seen after 7 and 14 days of healing. Cortical bone bridging of bone defect edges (BV/TV) was higher in experimental group (20.58 ±2.27) compared with the control (12.70 ±1.89). Detailed microCT analyses on bone microarchitecture are available in supplementary information (**Table 3.S1 and Table 3.S2**). Calcified specimens (n=3) were embedded in MMA, sectioned (5 □m), stained with Von Kossa and counterstained with MacNeal Tetrachrome. Von Kossa staining reveals some mineral deposits along with fibrous tissue as well as the remains of the surgifoam in the defects (**Fig. 3.2K-L**). The dynamic histomorphometry analysis on fluorochrome-labeled sections (Calcein and Alizarin Red) after 4 weeks postoperative (n=3) (**Fig. 3.2O-P**) shows a higher MS/BS ratio in the Tideglusib-treated group (11.23 ± 0.82) compared with control (7.91 ±0.82; p=0.001) (**Fig. 3.2Q**). MAR was significantly different between both groups (Control: 5.41 ±0.56; Tideglusib: 6.06 ±0.48; p=0.03) (**Fig. 3.2R**). The BFR/BS ratio was significantly increased in Tideglusib-treated defect group (2.73±0.13) compared to the control defect group (1.56±0.2; p=0.04) (**Fig. 3.1S**).

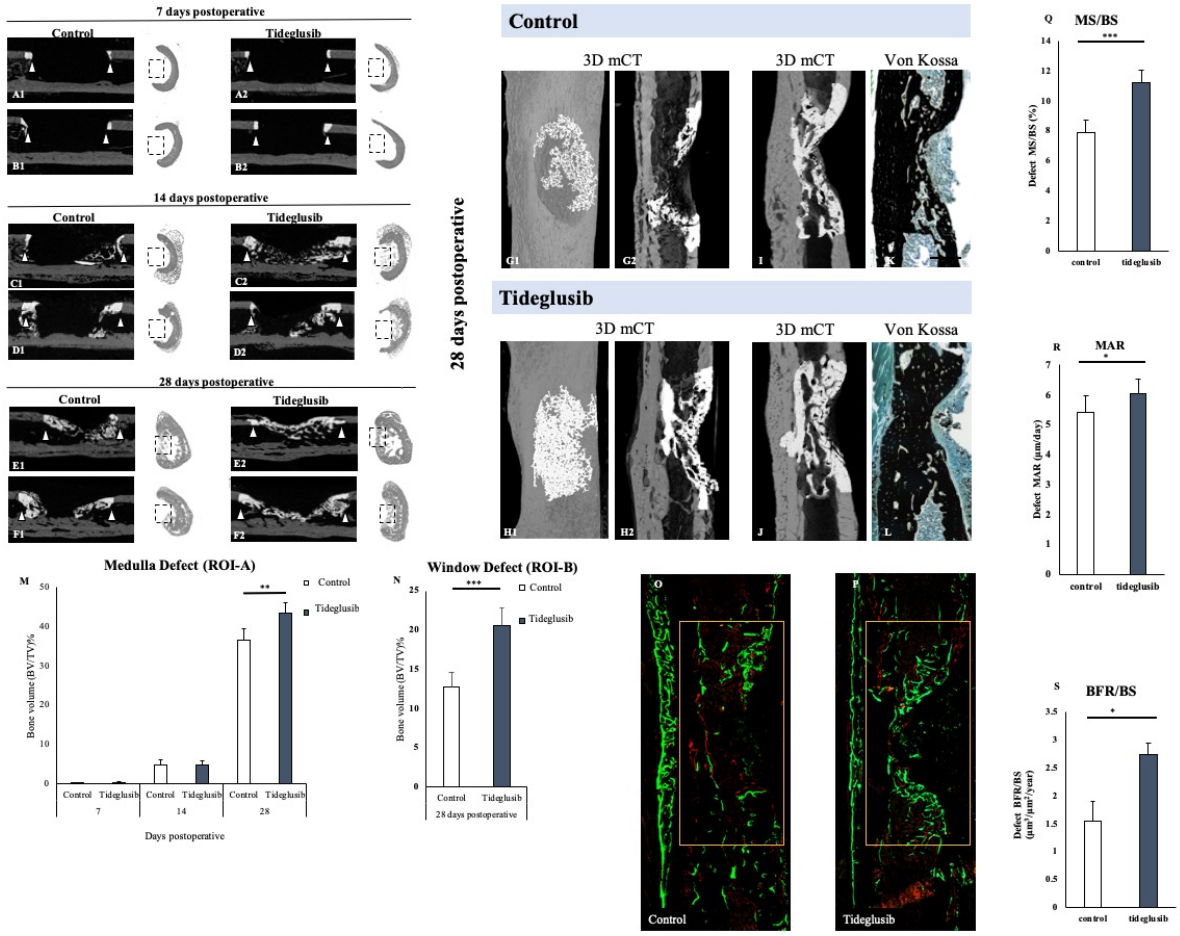

Figure 3.2. Radiologic and histologic analyses of bone repair.

Representative longitudinal and transversal microcomputed tomography (microCT) sections (**A-J**), plastic embedded calcified bone stained with Von Kossa (**K-L**) and double labeling with Calcein and Alizarin Red (**O-P**) images from paired femora are shown at 7 days (**A-B**), 14 days (**C-D**) and 28 days postoperative (**E-J**). Significant new bone formation (white) is seen after 28 days postoperative in the medulla (region of interest [ROI]-A) and cortical window defect (ROI-B). MicroCT analysis of medulla defect (ROI-A) is shown in left graph (**M**). The black dotted line delineates the 1.5mm x 0.9mm x 0.25mm ROI-B for the quantitative microCT analysis. Results after 28 days postoperative are displayed in right graph (**N**). Representative images of control (**O**) and Tideglusib-treated (**P**) defect labeled with Calcein (green; day 18) and Alizarin Red (red; day

25) were harvested at day 28 post-operative. Yellow line corresponds to the perimeter of the defect area. Specimens were labeled with a 7-day labeling period and Mineralizing surface/Bone surface (MS/BS), Mineral Apposition Rate (MAR), and Bone Formation Rate (BFR/BS) were calculated and are displayed in graphs on the right (**Q-S**). Images for fluorochrome double labeling are representative of n=3 specimens/experimental group/time-point. Tideglusib significantly different from control at * $p<0.05$, ** $p<0.01$ and ***$p<0.001$ at a given time-point. Scale bars = 500 μm (K-L).

Histological Analysis

Adjacent sections were stained for general morphological assessment (H&E), osteoblast activity (alkaline phosphatase, ALP) and presence of osteoclasts (tartrate resistant acid phosphatase, TRAP). Dense fibrous connective tissue, indicating the presence of the sponge, partially fills the defect at POD-7 (**Fig. 3.3A1-A2**) and POD-14 (**Fig. 3.3B1-B2**) with no attempt to bridge the bone defect area. However, the beginning of a medullary callus can be observed in the POD-14 defects. At POD-28, the defect area seems narrower in the Tideglusib-treated femora (**Fig. 3.3C2**), which matches the microCT results, whereas disorganized trabeculae can be seen in the control defects (**Fig. 3.3C1**). At POD-7 and POD-14, TRAP staining showed no significant difference between experimental and control groups (**Fig. 3.3G-H**). However, at POD-28, the presence of osteoclasts was more pronounced in the defect area of the control group (2.2 ±0.7) (**Fig. 3.3I1**) than the experimental group (1.3 ±0.4, p=0.04) (**Fig. 3.3I2**). ALP activity was similarly low in both groups at POD-7 (**Fig. 3.3J1-J2**) and increased in both experimental and control defects at POD-14 (**Fig. 3.3K1-K2**). The experimental group exhibits a higher ALP activity (1.8 ±0.3) than the control

(1.2 ±0.3, p=0.03). At POD-28, ALP activity in the experimental group drops significantly (0.47 ±0.05) (**Fig. 3.3L2**), while control becomes higher (1.0 ±0.2, p=0.02) (**Fig. 3.3L1**).

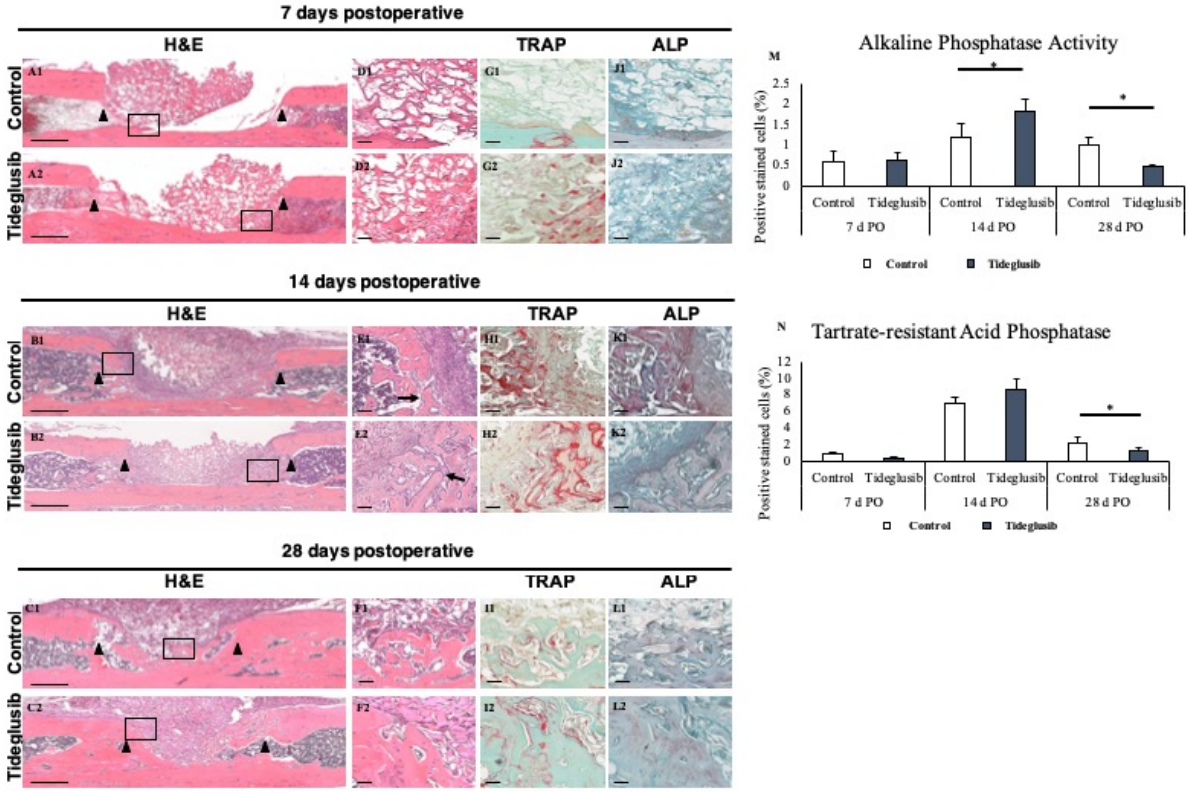

Figure 3.3. Histological analysis of bone repair. Representatives images of 5-µm sections from the mid-sagittal region of decalcified, paraffin embedded femurs were stained with hematoxylin and eosin (H&E) (**A-F**), and adjacent sections stained for TRAP to identify osteoclasts (**G-I**) and for ALP to identify osteoblasts (**J-L**). Low-magnification images of H&E stained sections show the margins of the defect (arrowheads) and the region of tissue (box) where high- magnification images were taken. At postoperative day (POD)-7, the defects are filled with dense fibrous tissue (**A1-A2**) whereas the formation of a medullary callus can be seen in defects at POD-14 (B1-B2). In the Tideglusib-treated femora, a clear trabecular pattern can be observed (**E2**) and to a lesser extent, also in the control defect (**E1**) (arrows). At 4 weeks postoperative, the bone defect area

appears narrower in the Tideglusib-treated femora (**C2**) when compared to the control (**C1**), where a disorganized trabecular pattern can be observed. Peak ALP activity was achieved at POD-14 in the experimental group (**K2**) and declined at POD-28 (**L2**), whereas control group achieved its peak activity later than the experimental at POD-28 (**L1**). Results for ALP activity for each end-point are shown in upper right graph (**M**). Osteoclast number was higher at POD-28 in the control group (**I1**) when compared with experimental defects (**I2**). POD-7 and POD-14 did not reach statistical significance, results are displayed in lower right graph (**N**). Tideglusib significantly different from control at *p<0.05 at a given time-point. Scale bars = 100 μm (**A-C**), 50 μm (**D-L**).

Immunohistochemistry

Immunohistochemistry for total GSK3β (total), pGSK3β-Tyr216 (active), and non-phospho(active)-β-catenin was performed. The results show that total GSK3β achieved its peak expression at POD-7 for both groups, however, the immunoreactivity in Tideglusib-treated femora (28.6 ±3.9) was higher than that of the control (22.6±3.2; p=0.047). The level of GSK3 β expression subsequently declined at POD-14 and POD-28 for both groups at comparable levels (**Fig. 3.4D-F**). At the early phase of bone healing, POD-7 and POD-14, the levels of the active form of the protein (pGSK3β-Tyr216) in the experimental group (POD7: 3.8 ±1.4; POD14: 16.9 ±5.6) were significantly lower than in the control group (POD7: 5.3 ±1.7; POD14: 23.5 ±6.9) (p=0.049 and p=0.036, respectively) (**Fig. 3.4G-I**). The levels for the active form afterwards declined at POD-28 (control: 6.4 ±1.9; Tideglusib: 8.0 ±3.2; p=0.78) and were comparable to those at POD-7. Despite no significant differences in the level of active β-catenin in the experimental (POD7: 1.6 ±0.3; POD28: 1.6 ±0.5) and control groups (POD7: 2.5 ±0.9; POD28: 1.9 ±0.8) at day 7 and 28 of healing, at POD-14 the experimental group (2.5±0.3) was significantly higher

than the control group (1.1±0.2, p=0.025) (**Fig. 3.4K1-K2**). Detailed histochemical and immunohistochemistry analysis is available in supplementary information (**Table 3.S3**).

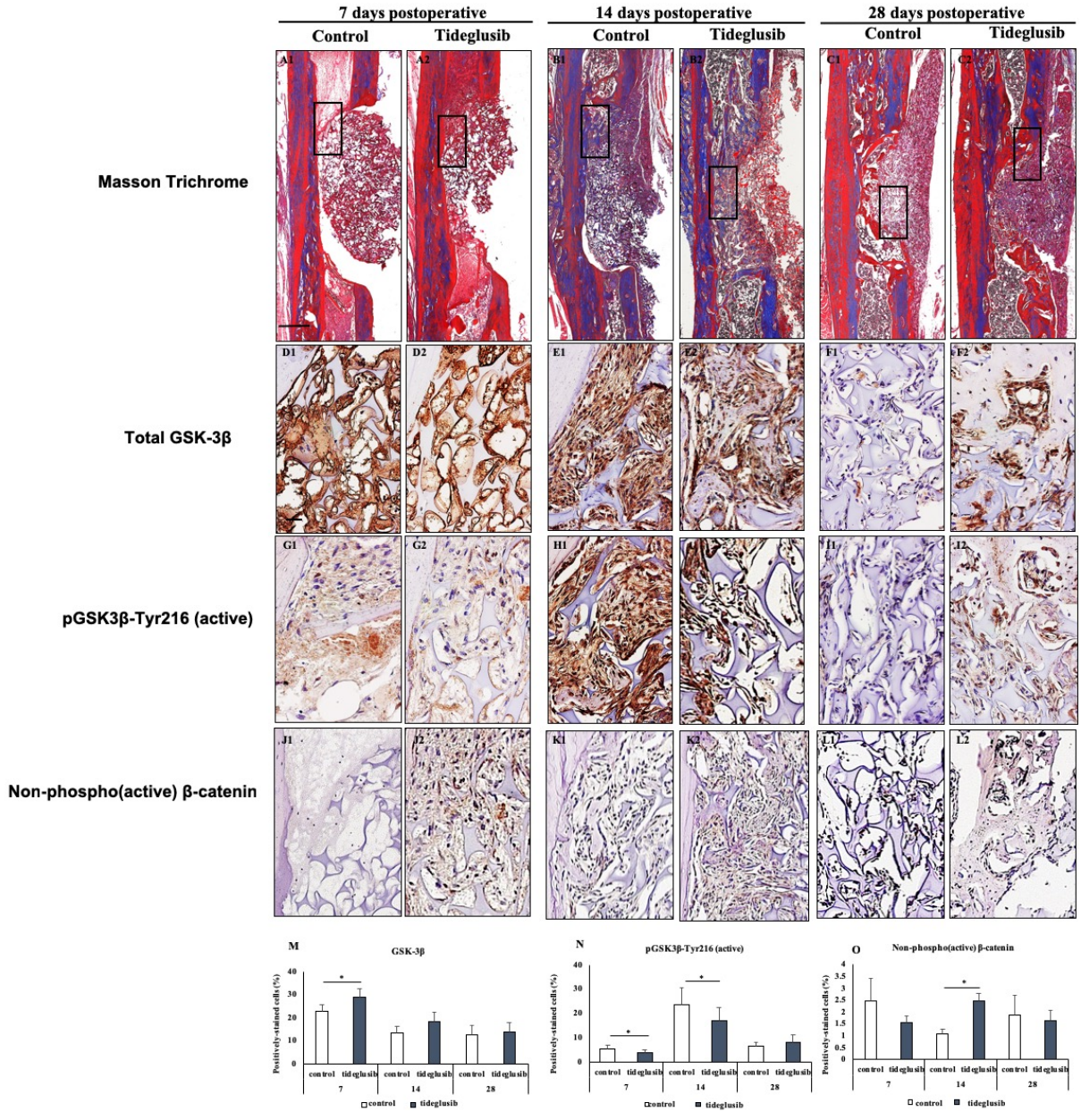

Figure 3.4. Immunohistochemical staining for evaluation of activation of Wnt/β-catenin signaling pathway in bone defect repair. Adjacent sections were stained with Masson trichome (**A-C**) and immunohistochemistry analysis for Wnt/ β-catenin pathway assessment was

performed. Representatives images of total GSK3β (**D-F**), pGSK3β-Tyr216 (active) (**G-I**), and non-phosphor(active) β-catenin (**J-L**). The levels of total GSK3β declined from POD-7 to POD-28, however the activity was always higher in the experimental group and was statistically significant at POD-7 only (**D1-D2**). On the contrary, immunoreactivity with pGSK3β-Tyr216 (active form of GSK3β) was significantly lower for Tideglusib-treated femora at POD-7 and POD-14. No difference was found at POD-28 in both groups. Quantitative analysis is shown in graphs below (**M-O**). Tideglusib significantly different from control at *$p<0.05$ at a given time-point. Scale bars = 500 μm (**A-C**), 50 μm (**D-L**).

3.6 Discussion

The objective of this study was to assess the impact of the localized delivery of Tideglusib on bone repair. Our results show enhanced bone healing after 28 days in a rodent model of intramembranous bone defect repair. The increase in BV/TV found on microCT at 28 days PO was preceded by an early peak in ALP activity at 14 days postoperative in the experimental group, suggesting an enhanced osteoblast differentiation in the Tideglusib group compared to the control group. Additionally, this upregulation was matched with an increase in bone mineralized content, as shown by an elevated MAR and BFR calculated by double-labeling at day 18 and day 25, which are both indictors of the rate of activity of matrix-producing osteoblasts (*265*). Taken together, our findings suggest a beneficial impact of the local administration of Tideglusib on bone repair.

Tideglusib is a non-reversible inhibitor of the constitutively active GSK-3β protein (*273*). The GSK-3β protein molecule is an inhibitor of bone formation within the Wnt signaling pathway. This pathway has been explored in recent years as part of the search for a specific molecule that could stabilize the crucial downstream target, β-catenin (*74*). Here, Tideglusib compared to control

group effectively downregulated active GSK-3β at POD-7 and POD-14 of the healing process, as well as upregulated β-catenin at 14 days postoperative. β-catenin then accumulates in the cytoplasm and translocates into the nucleus where it cooperates with Lef1/Tcf7 transcription factors to regulate gene expression of osteoblast differentiation and function (*53*). The findings of this study suggest that the early upregulation of osteoblast activity following stabilization of β-catenin by GSK-3β inhibition is likely the explanation of bone healing augmentation. Indeed, according to Chen et al, at day 9 and 14 post-fracture, β-catenin expression is at its highest (*192*). Being mostly expressed by osteoblasts during active bone repair (*274*), the increased expression of β-catenin at 14 days in the Tideglusib-treated femora coincides with a peak in ALP activity at 14 days. Taken together, these results suggest that the upregulation of mineralizing osteoblast activity is driven by overexpression of β-catenin leading to subsequent augmentation of bone defect healing. Additionally, control specimens display more ALP activity at POD-28, reinforcing the idea that Tideglusib-treated femora are further ahead in the healing process as osteoblast activity subsides when it becomes entrapped within the osteoid following increased quantity of matrix deposition (*235, 275*).

While the stimulatory effects of GSK-3β inhibition on bone enhancement have been demonstrated elsewhere with lithium chloride (LiCl) (*276, 277*), it is the first time that Tideglusib is used to accelerate bone regeneration. Knowing that short- and long-term toxicity of LiCl is a great concern (*278*), Tideglusib has proven to be safe in clinical trials for Alzheimer's disease (*279, 280*), and it is the only GSK inhibitor that has reached phase II trials (*281*). Chen et al. have shown that treatment with LiCl (*282*) only improves fracture healing when given after the inflammation stage (day 7) (*194*), once the mesenchymal cells have committed to become osteoblasts. They showed a deleterious effect when given before the fracture or too early, as LiCl caused an overexpression of

β-catenin in the early stages of bone healing and causes a blunting effect on osteoblasts (*192, 194, 283*). Contrary to this, the current results show that Tideglusib can safely be administered immediately upon creating the bone defect. Bearing in mind that the present study used a model of intramembranous repair, a repair process that starts with osteoblast differentiation from within mesenchymal cells condensation (*284*), the definitive role of Tideglusib on chondrocytes is not well understood and the use of a standard fracture model may or may not recapitulate the results observed following treatment with LiCl. However, this would be in line with Sisak et al.(*195*) where the use of a potent GSK-3 inhibitor was orally administered from day 1 post-fracture in rats, and did not replicate the altered bone healing pattern seen with LiCl treatment. Additionally, Arioka et al (*188*) found that after immediate local treatment with Li_2CO_3, bone healing was not impaired in a rodent model of intramembranous repair. With this study we aimed to evaluate skeletal progenitor cells recruitment and differentiation and here, osteoblast differentiation was clearly not affected compared to early β-catenin stabilizers treatment reporting impaired healing. This suggest that either Tideglusib, and other GSK-3ß inhibitors, operates differently than LiCl to induce bone healing, or that early activation of Wnt signaling pathway specifically for intramembranous ossification doesn't alter bone formation and development compared to endochondral ossification. These results highlight the fundamental differences of the role of Wnt/β-catenin signaling in intramembranous and endochondral bone repair. Hence, further studies on the mechanisms of the different GSK-3 inhibitors are required to understand how cells interact in the fracture site, towards intramembranous and endochondral ossification processes.

Although control defects exhibited a higher number of osteoclasts at POD-28, GSK-3β inhibition did not alter osteoclasts in the early phases of bone healing (POD-7 and POD-14) and was similar to the control. Several studies have suggested that inducing Wnt/β-catenin signaling (i.e. with

GSK-3β inhibition) would negatively regulates osteoclastogenesis by inducing secretion of osteoprotegerin (OPG), a well-known osteoclast inhibitor in terminally differentiated osteoblastic cells (*285-287*). However, a recent report has shown that GSK-3β inhibition suppresses osteoclasts differentiation of RAW264.7 cells independently of osteoblasts (*288*). This was further confirmed *in vivo* through a mouse model lacking β-catenin in the osteoclast lineage, leading to upregulation of bone resorption despite normal levels of OPG at 4 weeks (*288*). Our histological results reveal that Tideglusib delivered through a biodegradable collagen sponge directly applied to the bone defect successfully decreases the content of active GSK-3β, compared to control. This effect seems to last until at least POD-14, as active GSK-3β levels declined for both groups at POD-28. In the event of the drug being released in the next hours following collagen sponge insertion, instead of a supposed slow delivery caused by biodegradation of the collagen sponge, Tideglusib has shown to be an irreversible inhibitor of GSK-3β and combined with the low turnover rate of the enzyme, it may extend the duration of the pharmacological effect caused by this drug (*273*). Nevertheless, this study has demonstrated enhanced bone growth when Tideglusib was applied on the day of the surgery.

3.7 Acknowledgments

The research was supported by an Orthopedic Trauma Association resident grant. We thank the SAIL Technology Platform of the Research Institute of the McGill University for their support with the Zeiss AxioScan Z.1.

3.8 Supplementary information

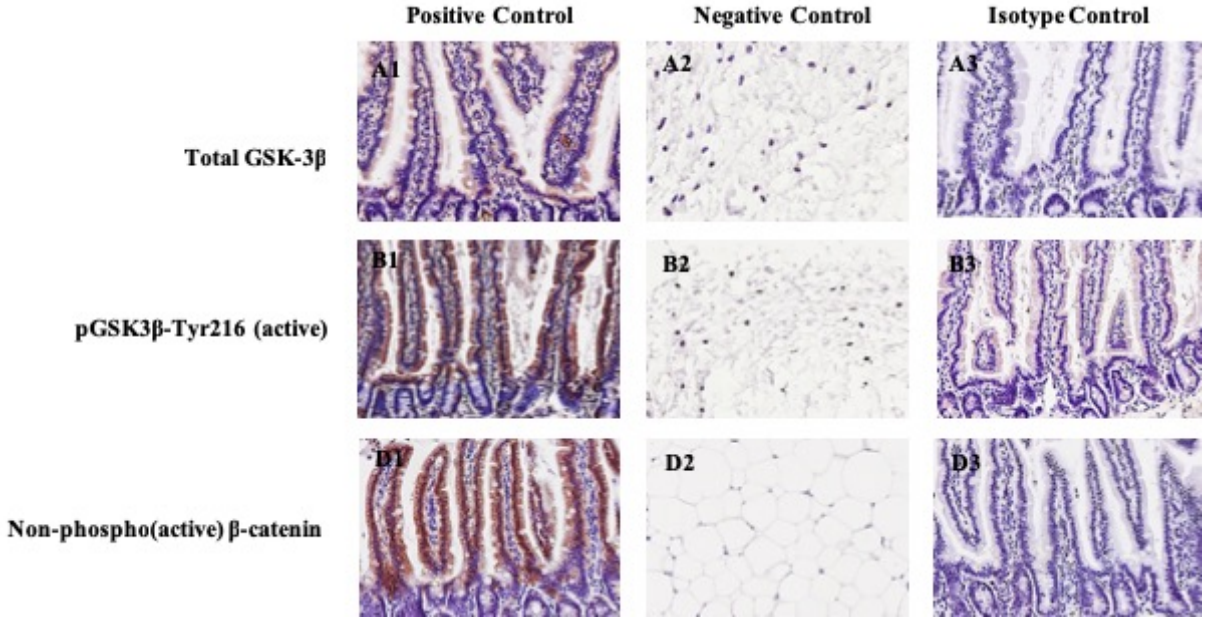

Figure 3.S1. Immunohistochemical staining of total GSK3β antibody (1:200, ab32391), phospho-Tyr216-GSK3β (pGSK3β-Tyr216) (1:50, ab75745, active form), and non-phospho(active)-β-catenin (Ser33/37/Thr41) (1:800, CST #8814) on normal mouse gastrointestinal tissue (positive control), mouse adipose tissue (negative control), and control isotype on same specimen as positive control.

Table 3.S1. Quantitative micro CT analysis of bone architecture of defect/medullary canal

	7 days postoperative			14 days postoperative			28 days postoperative		
	Control (n=11)	**Tidegl** (n=11)	**p value**	**Control** (n=12)	**Tidegl** (n=12)	**p value**	**Control** (n=12)	**Tidegl** (n=12)	**p value**
Medulla									
BV/TV %	0.04 ±0.02	0.35 ±0.25	0.240	4.76 ±1.22	4.82 ±0.86	0.973	36.53 ±2.88	43.31 ±2.67	**0.014**
Tb.Th. (μm)	0.02 ±0.0009	0.02 ±0.002	0.069	0.03 ±0.002	0.03 ±0.002	0.317	0.07 ±0.003	0.09 ±0.003	**0.0003**
Tb.Sp (μm)	0.65 ±0.03	0.65 ±0.03	0.903	0.39 ±0.04	0.03 ±0.002	**0.0001**	0.19 ±0.01	0.20 ±0.02	0.556
Po.Vop (mm^3)	0.95 ±0.003	0.94 ±0.002	0.268	0.25 ±0.01	0.15 ±0.03	**0.014**	0.62 ±0.03	0.55 ±0.03	**0.008**
Open Porosity (%)	99.96 ±0.02	99.87 ±0.07	0.236	73.55 ±4.0	63.91 ±4.2	**0.018**	63.43 ±2.89	56.64 ±2.68	**0.014**

BV/TV = bone volume/tissue volume; TbTh = trabecular thickness; TbSp. = trabecular separation; PoVop = open pore volume.

Table 3.S2. Quantitative micro CT analysis of bone architecture of window defect.

	28 days postoperative		
	Control	**Tidegl**	**p value**
	(n=12)	**(n=12)**	
Window Defect			
BV/TV %	12.7 ± 1.89	20.58 ± 2.27	**0.001**
Trabecular Number (No./ μm^3)	2.29 ± 0.99	3.27 ± 0.90	**0.004**
Tb.Th. (μm)	0.06 ± 0.01	0.06 ± 0.01	0.252
Tb.Sp (μm)	0.24 ± 0.07	0.24 ± 0.05	0.939
Closed Porosity (%)	0.08 ± 0.06	0.15 ± 0.12	**0.044**
Po.Vop (mm^3)	0.42 ± 0.03	0.38 ± 0.04	**0.002**
Open Porosity (%)	87.25 ± 6.54	79.38 ± 7.90	**<0.001**
Connective Density (μm^{-5})	6.58 ± 4.0	7.75 ± 4.0	0.494

BV/TV = bone volume/tissue volume; TbTh = trabecular thickness; TbSp. = trabecular separation; PoVop = open pore volume.

Table 3.S3. Quantitative staining analysis of cellular activity.

	7 days postoperative				14 days postoperative				28 days postoperative		
	Control	**Tidegl**	**p value**		**Control**	**Tidegl**	**p value**		**Control**	**Tidegl**	**p value**
ALP (%) (n=9)	0.65 ±0.2	0.63±0.2	0.944	ALP (%) (n=11)	1.2±0.3	1.8±0.2	**0.03**	ALP (%) (n=8)	1.0±0.2	0.47±0.05	**0.023**
TRAP (%) (n=9)	0.7±0.22	0.38±0.1	0.219	TRAP (%) (n=12)	6.5±0.7	6.8±1.2	0.847	TRAP (%) (n=9)	2.2±0.7	1.3±0.4	**0.043**
GSK-3β (%) (n=4)	22.6±3.2	28.6±3.9	**0.047**	GSK-3β (%) (n=4)	13.5±2.7	18.1±4.0	0.425	GSK-3β (%) (n=3)	12.6±4.0	14.0±3.9	0.860
pGSK3β-Tyr216 (%) (n=4)	5.3±1.7	3.8±1.4	**0.049**	pGSK3β-Tyr216 (%) (n=4)	23.5±6.9	16.9±5.6	**0.036**	pGSK3β-Tyr216 (%) (n=3)	6.4±1.9	8.0±3.2	0.776
(Active) β-catenin (%) (n=4)	2.5±0.9	1.6±0.3	0.47	(Active) β-catenin (%) (n=5)	1.1±0.2	2.5±0.3	**0.025**	(Active) β-catenin (%) (n=4)	1.9±0.8	1.6±0.5	0.84

ALP osteoblasts; TRAP osteoclasts;

CHAPTER 4. SUMMARY AND CONCLUSION

In our first paper, our results demonstrate that daily local cold therapy for 4 weeks accelerates/enhances bone healing in a murine model of intramembranous bone repair. To the best of our knowledge, our study is the first to investigate the effects of local cold therapy on bone healing. Further, our study suggests that this increase in osteogenesis may be mediated by the upregulation of the VEGF pathway due to intermittent cold induced hypoxia. Further studies exploring the mechanism of action of local cooling on bone healing, as well as the optimal treatment dose, duration, and frequency are warranted based on the results of this pilot study. If proven effective, local cold therapy can be introduced as a novel, cost effective, and non-invasive treatment modality to enhance bone healing in a clinical setting.

In our second paper, our study investigated the effects of local Tideglusib release, a known GSK-3β inhibitor, on a rodent model of bone defect repair. Early administration of Tideglusib promoted new bone formation via increased osteoblastic differentiation and mineralisation rate. Immunostaining showed a decrease in GSK-3β and an increase of β-catenin, which is known to positively regulate osteoblast differentiation and function. Additional work to unravel the effect of Tideglusib on osteoclast function and bone resorption during fracture healing is required. We strongly believe that this safe and FDA-approved drug has the potential to be used in the prevention of non-union in patients presenting with high risk for fracture-healing complications after optimisation of drug dose and treatment duration.

In conclusion, both studies demonstrated that two novel physical and chemical modalities, already FDA-approved, have been proven effective in acceleration of bone defect healing in the same

murine model of intramembranous healing. Further studies will be needed to determine their use as potential therapies for non-healing fractures or as adjuvants to other current modalities for enhancing critical-sized bone defect healing. Following the promising results from our first paper, our lab will develop a method for effective cold therapy delivery and funds were received for a small, proof-of-concept, clinical trial. Regarding the second paper, Tideglusib has the potential to be optimized as an orally delivered molecule as it has shown no toxicity in phase II clinical trials and would represent a great avenue towards systemic modalities for bone healing augmentation.

REFERENCES

1. G. Victoria, B. Petrisor, B. Drew, D. Dick, Bone stimulation for fracture healing: What's all the fuss? *Indian Journal of Orthopaedics* **43**, 117-120 (2009).
2. E. Gómez-Barrena *et al.*, Bone fracture healing: Cell therapy in delayed unions and nonunions. *Bone* **70**, 93-101 (2015).
3. C. Tzioupis, P. V. Giannoudis, Prevalence of long-bone non-unions. *Injury* **38**, S3-S9 (2007).
4. E. P. Fowler, P. M. Osmun, New bone growth due to cold water in the ears. *Archives of Otolaryngology* **36**, 455-466 (1942).
5. F. H. Linthicum Jr, T. A. Stewart Jr, Exostoses of the external auditory canal. *Otology & Neurotology* **26**, 1243-1244 (2005).
6. J. J. Patel *et al.*, Hypothermia inhibits osteoblast differentiation and bone formation but stimulates osteoclastogenesis. *Experimental cell research* **318**, 2237-2244 (2012).
7. J. J. Patel *et al.*, Hypothermia stimulates osteoclastogenesis but inhibits osteoblast differentiation and bone formation. *Bone* **44**, S305 (2009).
8. M. D. Aisha *et al.*, Short-term moderate hypothermia stimulates alkaline phosphatase activity and osteocalcin expression in osteoblasts by upregulating Runx2 and osterix in vitro. *Experimental cell research* **326**, 46-56 (2014).
9. V. C. Neves, R. Babb, D. Chandrasekaran, P. T. Sharpe, Promotion of natural tooth repair by small molecule GSK3 antagonists. *Sci Rep* **7**, 39654 (2017).
10. J. Westgeest *et al.*, Factors associated with development of nonunion or delayed healing after an open long bone fracture: a prospective cohort study of 736 subjects. *Journal of orthopaedic trauma* **30**, 149-155 (2016).
11. L. A. Mills, S. A. Aitken, A. H. R. W. Simpson, The risk of non-union per fracture: current myths and revised figures from a population of over 4 million adults. *Acta orthopaedica* **88**, 434-439 (2017).
12. D. J. Hak *et al.*, Delayed union and nonunions: epidemiology, clinical issues, and financial aspects. *Injury* **45 Suppl 2**, S3-7 (2014).
13. C. Copuroglu, G. M. Calori, P. V. Giannoudis, Fracture non-union: who is at risk? *Injury* **44**, 1379-1382 (2013).
14. Y. Wang, M. R. Newman, D. S. W. Benoit, Development of controlled drug delivery systems for bone fracture-targeted therapeutic delivery: A review. *Eur J Pharm Biopharm* **127**, 223-236 (2018).
15. R. Dimitriou, N. Kanakaris, P. N. Soucacos, P. V. Giannoudis, Genetic predisposition to non-union: evidence today. *Injury* **44 Suppl 1**, S50-53 (2013).
16. I. Pountos, T. Georgouli, S. Pneumaticos, P. V. Giannoudis, Fracture non-union: Can biomarkers predict outcome? *Injury* **44**, 1725-1732 (2013).
17. J. A. Bishop, A. A. Palanca, M. J. Bellino, D. W. Lowenberg, Assessment of compromised fracture healing. *J Am Acad Orthop Surg* **20**, 273-282 (2012).
18. G. M. Calori *et al.*, Non-unions. *Clinical cases in mineral and bone metabolism : the official journal of the Italian Society of Osteoporosis, Mineral Metabolism, and Skeletal Diseases* **14**, 186-188 (2017).
19. F. N. Kwong, M. B. Harris, Recent developments in the biology of fracture repair. *J Am Acad Orthop Surg* **16**, 619-625 (2008).

20. M. Ramachandran, *Basic orthopaedic sciences*. (CRC Press, 2018).
21. L. Claes, S. Recknagel, A. Ignatius, Fracture healing under healthy and inflammatory conditions. *Nat Rev Rheumatol* **8**, 133-143 (2012).
22. R. Dimitriou, E. Tsiridis, P. V. Giannoudis, Current concepts of molecular aspects of bone healing. *Injury* **36**, 1392-1404 (2005).
23. R. Marsell, T. A. Einhorn, The biology of fracture healing. *Injury* **42**, 551-555 (2011).
24. B. McKibbin, The biology of fracture healing in long bones. *The Journal of bone and joint surgery. British volume* **60**, 150-162 (1978).
25. T. J. Thompson, P. D. Owens, D. J. Wilson, Intramembranous osteogenesis and angiogenesis in the chick embryo. *J Anat* **166**, 55-65 (1989).
26. C. J. Percival, J. T. Richtsmeier, Angiogenesis and intramembranous osteogenesis. *Dev Dyn* **242**, 909-922 (2013).
27. T. P. Rüedi, W. M. Murphy, AO principles of fracture management. *Davos: AO Publishing & Stuttgart New York: Georg Thieme Verlag*, (2000).
28. H.-C. Pape, P. V. Giannoudis, K. Grimme, M. van Griensven, C. Krettek, Effects of intramedullary femoral fracture fixation: what is the impact of experimental studies in regards to the clinical knowledge? *Shock* **18**, 291-300 (2002).
29. S. M. Perren, Evolution of the internal fixation of long bone fractures: the scientific basis of biological internal fixation: choosing a new balance between stability and biology. *The Journal of bone and joint surgery. British volume* **84**, 1093-1110 (2002).
30. C. M. Runyan, K. S. Gabrick, Biology of Bone Formation, Fracture Healing, and Distraction Osteogenesis. *J Craniofac Surg* **28**, 1380-1389 (2017).
31. P. Kolar *et al.*, The early fracture hematoma and its potential role in fracture healing. *Tissue Engineering Part B: Reviews* **16**, 427-434 (2010).
32. J. B. Wray, Acute changes in femoral arterial blood flow after closed tibial fracture in dogs. *JBJS* **46**, 1262-1268 (1964).
33. P. Kolar, T. Gaber, C. Perka, G. N. Duda, F. Buttgereit, Human early fracture hematoma is characterized by inflammation and hypoxia. *Clin Orthop Relat Res* **469**, 3118-3126 (2011).
34. L. C. Gerstenfeld, D. M. Cullinane, G. L. Barnes, D. T. Graves, T. A. Einhorn, Fracture healing as a post-natal developmental process: Molecular, spatial, and temporal aspects of its regulation. *Journal of cellular biochemistry* **88**, 873-884 (2003).
35. Z. S. Ai-Aql, A. S. Alagl, D. T. Graves, L. C. Gerstenfeld, T. A. Einhorn, Molecular mechanisms controlling bone formation during fracture healing and distraction osteogenesis. *Journal of dental research* **87**, 107-118 (2008).
36. T. Kon *et al.*, Expression of osteoprotegerin, receptor activator of NF-kappaB ligand (osteoprotegerin ligand) and related proinflammatory cytokines during fracture healing. *J Bone Miner Res* **16**, 1004-1014 (2001).
37. J. Drager, E. J. Harvey, J. Barralet, Hypoxia signalling manipulation for bone regeneration. *Expert Rev Mol Med* **17**, e6 (2015).
38. G. L. Barnes, P. J. Kostenuik, L. C. Gerstenfeld, T. A. Einhorn, Growth factor regulation of fracture repair. *J Bone Miner Res* **14**, 1805-1815 (1999).
39. T. A. Einhorn, The science of fracture healing. *J Orthop Trauma* **19**, S4-6 (2005).

40. T. A. Einhorn, The cell and molecular biology of fracture healing. *Clin Orthop Relat Res*, S7-21 (1998).
41. A. M. Phillips, Overview of the fracture healing cascade. *Injury* **36 Suppl 3**, S5-7 (2005).
42. L. C. Gerstenfeld *et al.*, Three-dimensional reconstruction of fracture callus morphogenesis. *J Histochem Cytochem* **54**, 1215-1228 (2006).
43. M. Melnyk, T. Henke, L. Claes, P. Augat, Revascularisation during fracture healing with soft tissue injury. *Arch Orthop Trauma Surg* **128**, 1159-1165 (2008).
44. F. W. Rhinelander, Tibial blood supply in relation to fracture healing. *Clin Orthop Relat Res*, 34-81 (1974).
45. L. Claes, K. Eckert-Hubner, P. Augat, The effect of mechanical stability on local vascularization and tissue differentiation in callus healing. *J Orthop Res* **20**, 1099-1105 (2002).
46. L. Claes *et al.*, Monitoring and healing analysis of 100 tibial shaft fractures. *Langenbecks Arch Surg* **387**, 146-152 (2002).
47. Q. Wang, C. Huang, F. Zeng, M. Xue, X. Zhang, Activation of the Hh pathway in periosteum-derived mesenchymal stem cells induces bone formation in vivo: implication for postnatal bone repair. *Am J Pathol* **177**, 3100-3111 (2010).
48. S. Minear *et al.*, Wnt proteins promote bone regeneration. *Sci Transl Med* **2**, 29ra30 (2010).
49. Y. Komiya, R. Habas, Wnt signal transduction pathways. *Organogenesis* **4**, 68-75 (2008).
50. X. He, M. Semenov, K. Tamai, X. Zeng, LDL receptor-related proteins 5 and 6 in Wnt/beta-catenin signaling: arrows point the way. *Development* **131**, 1663-1677 (2004).
51. J. B. Wallingford, R. Habas, The developmental biology of Dishevelled: an enigmatic protein governing cell fate and cell polarity. *Development* **132**, 4421-4436 (2005).
52. S. Hatsell, T. Rowlands, M. Hiremath, P. Cowin, Beta-catenin and Tcfs in mammary development and cancer. *J Mammary Gland Biol Neoplasia* **8**, 145-158 (2003).
53. H. Clevers, Wnt/beta-catenin signaling in development and disease. *Cell* **127**, 469-480 (2006).
54. T. Reya, H. Clevers, Wnt signalling in stem cells and cancer. *Nature* **434**, 843-850 (2005).
55. W. Wu, A. Glinka, H. Delius, C. Niehrs, Mutual antagonism between dickkopf1 and dickkopf2 regulates Wnt/beta-catenin signalling. *Curr Biol* **10**, 1611-1614 (2000).
56. J. C. Hsieh *et al.*, A new secreted protein that binds to Wnt proteins and inhibits their activities. *Nature* **398**, 431-436 (1999).
57. A. Uren *et al.*, Secreted frizzled-related protein-1 binds directly to Wingless and is a biphasic modulator of Wnt signaling. *J Biol Chem* **275**, 4374-4382 (2000).
58. S. Piccolo *et al.*, The head inducer Cerberus is a multifunctional antagonist of Nodal, BMP and Wnt signals. *Nature* **397**, 707-710 (1999).
59. S. Wang, M. Krinks, K. Lin, F. P. Luyten, M. Moos, Jr., Frzb, a secreted protein expressed in the Spemann organizer, binds and inhibits Wnt-8. *Cell* **88**, 757-766 (1997).
60. M. Semenov, K. Tamai, X. He, SOST is a ligand for LRP5/LRP6 and a Wnt signaling inhibitor. *J Biol Chem* **280**, 26770-26775 (2005).
61. Q. Xu *et al.*, Vascular development in the retina and inner ear: control by Norrin and Frizzled-4, a high-affinity ligand-receptor pair. *Cell* **116**, 883-895 (2004).

62. O. Kazanskaya *et al.*, R-Spondin2 is a secreted activator of Wnt/beta-catenin signaling and is required for Xenopus myogenesis. *Dev Cell* **7**, 525-534 (2004).
63. Y. Kawano, R. Kypta, Secreted antagonists of the Wnt signalling pathway. *J Cell Sci* **116**, 2627-2634 (2003).
64. K. J. Escott, P. J. O'Shea, The role of glycogen synthase kinase-3 inhibitors on bone remodeling. *The Biology and Therapeutic Application of Mesenchymal Cells*, 148-166 (2016).
65. K. Takemaru *et al.*, Chibby, a nuclear beta-catenin-associated antagonist of the Wnt/Wingless pathway. *Nature* **422**, 905-909 (2003).
66. O. O. Piven, C. L. Winata, The canonical way to make a heart: beta-catenin and plakoglobin in heart development and remodeling. *Exp Biol Med (Maywood)* **242**, 1735-1745 (2017).
67. M. Lehmann, H. A. Baarsma, M. Konigshoff, WNT Signaling in Lung Aging and Disease. *Ann Am Thorac Soc* **13 Suppl 5**, S411-s416 (2016).
68. M. Hussain, C. Xu, M. Lu, X. Wu, L. Tang, Wnt/beta-catenin signaling links embryonic lung development and asthmatic airway remodeling. *Biochim Biophys Acta Mol Basis Dis* **1863**, 3226-3242 (2017).
69. Y. Zuo, Y. Liu, New insights into the role and mechanism of Wnt/beta-catenin signalling in kidney fibrosis. *Nephrology (Carlton)* **23 Suppl 4**, 38-43 (2018).
70. K. Nishikawa, Y. Osawa, K. Kimura, Wnt/beta-Catenin Signaling as a Potential Target for the Treatment of Liver Cirrhosis Using Antifibrotic Drugs. *Int J Mol Sci* **19**, (2018).
71. A. W. Burgess, M. C. Faux, M. J. Layton, R. G. Ramsay, Wnt signaling and colon tumorigenesis--a view from the periphery. *Exp Cell Res* **317**, 2748-2758 (2011).
72. Y. Wang *et al.*, Wnt and the Wnt signaling pathway in bone development and disease. *Front Biosci (Landmark Ed)* **19**, 379-407 (2014).
73. J. B. Kim *et al.*, Bone regeneration is regulated by wnt signaling. *J Bone Miner Res* **22**, 1913-1923 (2007).
74. H. Xu *et al.*, Role of Wnt signaling in fracture healing. *BMB reports* **47**, 666 (2014).
75. C. Y. Logan, R. Nusse, The Wnt signaling pathway in development and disease. *Annu Rev Cell Dev Biol* **20**, 781-810 (2004).
76. P. V. Giannoudis, T. A. Einhorn, D. Marsh, Fracture healing: the diamond concept. *Injury* **38**, S3-S6 (2007).
77. H. M. Frost, Skeletal structural adaptations to mechanical usage (SATMU): 1. Redefining Wolff's law: the bone modeling problem. *The Anatomical Record* **226**, 403-413 (1990).
78. S. M. Perren, Physical and biological aspects of fracture healing with special reference to internal fixation. *Clin Orthop Relat Res*, 175-196 (1979).
79. R. Leighton *et al.*, Healing of fracture nonunions treated with low-intensity pulsed ultrasound (LIPUS): A systematic review and meta-analysis. *Injury* **48**, 1339-1347 (2017).
80. P. A. Nolte *et al.*, Low-intensity pulsed ultrasound in the treatment of nonunions. *J Trauma* **51**, 693-702; discussion 702-693 (2001).
81. D. Gebauer, E. Mayr, E. Orthner, J. P. Ryaby, Low-intensity pulsed ultrasound: effects on nonunions. *Ultrasound Med Biol* **31**, 1391-1402 (2005).
82. B. Biglari *et al.*, Failed treatment of long bone nonunions with low intensity pulsed ultrasound. *Arch Orthop Trauma Surg* **136**, 1121-1134 (2016).

83. S. Rutten, M. P. van den Bekerom, I. N. Sierevelt, P. A. Nolte, Enhancement of Bone-Healing by Low-Intensity Pulsed Ultrasound: A Systematic Review. *JBJS Rev* **4**, (2016).
84. J. W. Busse *et al.*, Low intensity pulsed ultrasonography for fractures: systematic review of randomised controlled trials. *Bmj* **338**, b351 (2009).
85. X. L. Griffin, N. Parsons, M. L. Costa, D. Metcalfe, Ultrasound and shockwave therapy for acute fractures in adults. *Cochrane Database Syst Rev*, Cd008579 (2014).
86. P. F. Hannemann, E. H. Mommers, J. P. Schots, P. R. Brink, M. Poeze, The effects of low-intensity pulsed ultrasound and pulsed electromagnetic fields bone growth stimulation in acute fractures: a systematic review and meta-analysis of randomized controlled trials. *Arch Orthop Trauma Surg* **134**, 1093-1106 (2014).
87. W. G. de Haas, J. Watson, D. M. Morrison, Non-invasive treatment of ununited fractures of the tibia using electrical stimulation. *J Bone Joint Surg Br* **62-b**, 465-470 (1980).
88. H. F. Shi *et al.*, Early application of pulsed electromagnetic field in the treatment of postoperative delayed union of long-bone fractures: a prospective randomized controlled study. *BMC Musculoskelet Disord* **14**, 35 (2013).
89. C. A. Bassett, S. N. Mitchell, S. R. Gaston, Treatment of ununited tibial diaphyseal fractures with pulsing electromagnetic fields. *J Bone Joint Surg Am* **63**, 511-523 (1981).
90. W. J. Sharrard, M. L. Sutcliffe, M. J. Robson, A. G. Maceachern, The treatment of fibrous non-union of fractures by pulsing electromagnetic stimulation. *J Bone Joint Surg Br* **64**, 189-193 (1982).
91. A. T. Barker, R. A. Dixon, W. J. Sharrard, M. L. Sutcliffe, Pulsed magnetic field therapy for tibial non-union. Interim results of a double-blind trial. *Lancet* **1**, 994-996 (1984).
92. W. G. de Haas, A. Beaupre, H. Cameron, E. English, The Canadian experience with pulsed magnetic fields in the treatment of ununited tibial fractures. *Clin Orthop Relat Res*, 55-58 (1986).
93. G. Scott, J. B. King, A prospective, double-blind trial of electrical capacitive coupling in the treatment of non-union of long bones. *J Bone Joint Surg Am* **76**, 820-826 (1994).
94. R. B. Simonis, E. J. Parnell, P. S. Ray, J. L. Peacock, Electrical treatment of tibial non-union: a prospective, randomised, double-blind trial. *Injury* **34**, 357-362 (2003).
95. A. K. Gupta, K. P. Srivastava, S. Avasthi, Pulsed electromagnetic stimulation in nonunion of tibial diaphyseal fractures. *Indian J Orthop* **43**, 156-160 (2009).
96. S. Adie *et al.*, Pulsed electromagnetic field stimulation for acute tibial shaft fractures: a multicenter, double-blind, randomized trial. *J Bone Joint Surg Am* **93**, 1569-1576 (2011).
97. A. Assiotis, N. P. Sachinis, B. E. Chalidis, Pulsed electromagnetic fields for the treatment of tibial delayed unions and nonunions. A prospective clinical study and review of the literature. *J Orthop Surg Res* **7**, 24 (2012).
98. F. a. D. Administration, F. a. D. Administration, Ed. (US, 2004).
99. B. Mollon, V. da Silva, J. W. Busse, T. A. Einhorn, M. Bhandari, Electrical stimulation for long-bone fracture-healing: a meta-analysis of randomized controlled trials. *J Bone Joint Surg Am* **90**, 2322-2330 (2008).
100. M. Griffin, A. Bayat, Electrical stimulation in bone healing: critical analysis by evaluating levels of evidence. *Eplasty* **11**, e34 (2011).

101. X. L. Griffin, M. L. Costa, N. Parsons, N. Smith, Electromagnetic field stimulation for treating delayed union or non-union of long bone fractures in adults. *Cochrane Database Syst Rev* **4**, (2011).
102. L. Brosseau *et al.*, Thermotherapy for treatment of osteoarthritis. *The Cochrane Library*, (2003).
103. M. C. Raynor, R. Pietrobon, U. Guller, L. D. Higgins, Cryotherapy after ACL reconstruction: a meta-analysis. *J Knee Surg* **18**, 123-129 (2005).
104. D. C. Mac Auley, Ice therapy: how good is the evidence? *Int J Sports Med* **22**, 379-384 (2001).
105. X. Guillot *et al.*, Cryotherapy in inflammatory rheumatic diseases: a systematic review. *Expert Rev Clin Immunol* **10**, 281-294 (2014).
106. G. A. Malanga, N. Yan, J. Stark, Mechanisms and efficacy of heat and cold therapies for musculoskeletal injury. *Postgrad Med* **127**, 57-65 (2015).
107. C. Bleakley *et al.*, Cold-water immersion (cryotherapy) for preventing and treating muscle soreness after exercise. *Cochrane Database Syst Rev*, Cd008262 (2012).
108. S. Adie, A. Kwan, J. M. Naylor, I. A. Harris, R. Mittal, Cryotherapy following total knee replacement. *The Cochrane database of systematic reviews* **9**, (2012).
109. S. H. Ni *et al.*, Cryotherapy on postoperative rehabilitation of joint arthroplasty. *Knee Surg Sports Traumatol Arthrosc* **23**, 3354-3361 (2015).
110. J. S. Petrofsky *et al.*, The influence of local versus global heat on the healing of chronic wounds in patients with diabetes. *Diabetes Technol Ther* **9**, 535-544 (2007).
111. J. M. Rabkin, T. K. Hunt, Local heat increases blood flow and oxygen tension in wounds. *Arch Surg* **122**, 221-225 (1987).
112. S. F. Nadler, K. Weingand, R. J. Kruse, The physiologic basis and clinical applications of cryotherapy and thermotherapy for the pain practitioner. *Pain physician* **7**, 395-400 (2004).
113. C. M. Bleakley, J. T. Costello, Do thermal agents affect range of movement and mechanical properties in soft tissues? A systematic review. *Arch Phys Med Rehabil* **94**, 149-163 (2013).
114. M. Hardy, W. Woodall, Therapeutic effects of heat, cold, and stretch on connective tissue. *J Hand Ther* **11**, 148-156 (1998).
115. T. Rosenbaum, S. A. Simon, in *TRP Ion Channel Function in Sensory Transduction and Cellular Signaling Cascades,* W. B. Liedtke, S. Heller, Eds. (CRC Press/Taylor & Francis Taylor & Francis Group, LLC., Boca Raton (FL), 2007).
116. M. M. Moran, M. A. McAlexander, T. Biro, A. Szallasi, Transient receptor potential channels as therapeutic targets. *Nat Rev Drug Discov* **10**, 601-620 (2011).
117. C. Ficat, in *Bone Circulation and Bone Necrosis*. (Springer, 1990), pp. 389-394.
118. W. M. Eagleson, K. I. Deckert, E. E. Townsend, J. R. Arnott, The effect of heat on the healing of fractures: a preliminary experimental report. *Canadian Medical Association Journal* **97**, 274 (1967).
119. S. A. Leon *et al.*, Effects of hyperthermia on bone. II. Heating of bone in vivo and stimulation of bone growth. *Int J Hyperthermia* **9**, 77-87 (1993).
120. K. Ikuta *et al.*, In vivo heat-stimulus-triggered osteogenesis. *Int J Hyperthermia* **31**, 58-66 (2015).

121. R. Wootton, P. Jennings, C. King-Underwood, S. J. Wood, The effect of intermittent local heating on fracture healing in the distal tibia of the rabbit. *International orthopaedics* **14**, 189-193 (1990).
122. T. Ota *et al.*, Heat-stimuli-enhanced osteogenesis using clinically available biomaterials. *PLoS One* **12**, e0181404 (2017).
123. W. H. Chang, J. S. Sun, S. P. Chang, J. C. Lin, Study of thermal effects of ultrasound stimulation on fracture healing. *Bioelectromagnetics* **23**, 256-263 (2002).
124. K. P. Speer, R. F. Warren, L. Horowitz, The efficacy of cryotherapy in the postoperative shoulder. *Journal of shoulder and elbow surgery* **5**, 62-68 (1996).
125. M. G. Dolan, R. M. Thornton, D. R. Fish, F. C. Mendel, Effects of cold water immersion on edema formation after blunt injury to the hind limbs of rats. *J Athl Train* **32**, 233-237 (1997).
126. A. A. Algafly, K. P. George, The effect of cryotherapy on nerve conduction velocity, pain threshold and pain tolerance. *British journal of sports medicine* **41**, 365-369 (2007).
127. D. I. Abramson *et al.*, Effect of tissue temperatures and blood flow on motor nerve conduction velocity. *Jama* **198**, 1082-1088 (1966).
128. W. Gregson *et al.*, Influence of cold water immersion on limb and cutaneous blood flow at rest. *Am J Sports Med* **39**, 1316-1323 (2011).
129. H. Lee *et al.*, Effects of cryotherapy after contusion using real-time intravital microscopy. *Medicine and science in sports and exercise* **37**, 1093-1098 (2005).
130. S. Khoshnevis, N. K. Craik, R. Matthew Brothers, K. R. Diller, Cryotherapy-Induced Persistent Vasoconstriction After Cutaneous Cooling: Hysteresis Between Skin Temperature and Blood Perfusion. *Journal of biomechanical engineering* **138**, 4032126 (2016).
131. S. S. Ho, M. N. Coel, R. Kagawa, A. B. Richardson, The effects of ice on blood flow and bone metabolism in knees. *Am J Sports Med* **22**, 537-540 (1994).
132. C. Taber, K. Contryman, J. Fahrenbruch, K. LaCount, M. W. Cornwall, Measurement of reactive vasodilation during cold gel pack application to nontraumatized ankles. *Phys Ther* **72**, 294-299 (1992).
133. D. N. Deal, J. Tipton, E. Rosencrance, W. W. Curl, T. L. Smith, Ice reduces edema. A study of microvascular permeability in rats. *J Bone Joint Surg Am* **84-a**, 1573-1578 (2002).
134. K. D. Schaser *et al.*, In vivo analysis of microcirculation following closed soft-tissue injury. *J Orthop Res* **17**, 678-685 (1999).
135. K. D. Schaser *et al.*, Prolonged superficial local cryotherapy attenuates microcirculatory impairment, regional inflammation, and muscle necrosis after closed soft tissue injury in rats. *Am J Sports Med* **35**, 93-102 (2007).
136. K. D. Schaser *et al.*, Local cooling restores microcirculatory hemodynamics after closed soft-tissue trauma in rats. *The Journal of trauma* **61**, 642-649 (2006).
137. S. Westermann, B. Vollmar, H. Thorlacius, M. D. Menger, Surface cooling inhibits tumor necrosis factor-alpha-induced microvascular perfusion failure, leukocyte adhesion, and apoptosis in the striated muscle. *Surgery* **126**, 881-889 (1999).
138. C. M. Bleakley, P. Glasgow, M. J. Webb, Cooling an acute muscle injury: can basic scientific theory translate into the clinical setting? *Br J Sports Med* **46**, 296-298 (2012).

139. A. A. Sapega *et al.*, The bioenergetics of preservation of limbs before replantation. The rationale for intermediate hypothermia. *J Bone Joint Surg Am* **70**, 1500-1513 (1988).
140. A. L. Osterman *et al.*, Muscle ischemia and hypothermia: a bioenergetic study using 31phosphorus nuclear magnetic resonance spectroscopy. *J Trauma* **24**, 811-817 (1984).
141. M. A. Merrick, J. M. Rankin, F. A. Andres, C. L. Hinman, A preliminary examination of cryotherapy and secondary injury in skeletal muscle. *Med Sci Sports Exerc* **31**, 1516-1521 (1999).
142. C. M. Bleakley, S. M. McDonough, D. C. MacAuley, J. Bjordal, Cryotherapy for acute ankle sprains: a randomised controlled study of two different icing protocols. *Br J Sports Med* **40**, 700-705; discussion 705 (2006).
143. J. Haines, A survey of recent developments in cold therapy. *Physiotherapy* **53**, 222-229 (1967).
144. C. Swenson, L. Sward, J. Karlsson, Cryotherapy in sports medicine. *Scandinavian journal of medicine & science in sports* **6**, 193-200 (1996).
145. J. A. Allen, The influence of physical conditions in the genesis of species. *Radical review* **1**, 108-140 (1877).
146. M. A. Serrat, Environmental temperature impact on bone and cartilage growth. *Compr Physiol* **4**, 621-655 (2014).
147. L. Chevillard, R. Portet, M. Cadot. vol. 22, pp. 699.
148. F. Al-Hilli, E. A. Wright, The short term effects of a supra-lethal dose of irradiation and changes in the environmental temperature on the growth of tail bones of the mouse. *Br J Exp Pathol* **64**, 684-692 (1983).
149. M. A. E.-R. Ashoub, Effect of two extreme temperatures on growth and tail-length of mice. *Nature* **181**, 284 (1958).
150. M. M. Lee, P. C. Chu, H. C. Chan, Effects of cold on the skeletal growth of albino rats. *Am J Anat* **124**, 239-249 (1969).
151. C. Ogle, Climatic influence on the growth of the male albino mouse. *American Journal of Physiology-Legacy Content* **107**, 635-640 (1934).
152. M. A. Serrat, Allen's rule revisited: temperature influences bone elongation during a critical period of postnatal development. *Anat Rec (Hoboken)* **296**, 1534-1545 (2013).
153. M. A. Serrat, D. King, C. O. Lovejoy, Temperature regulates limb length in homeotherms by directly modulating cartilage growth. *Proc Natl Acad Sci U S A* **105**, 19348-19353 (2008).
154. M. A. Serrat, Environmentally-determined tissue temperature modulates extremity growth in mammals: A potential comprehensive explanation of Allen's rule. (2007).
155. M. E. Weaver, D. L. Ingram, Morphological changes in swine associated with environmental temperature. *Ecology* **50**, 710-713 (1969).
156. K. Horst *et al.*, Long-term effects of induced hypothermia on local and systemic inflammation-Results from a porcine long-term trauma model. *PloS one* **11**, e0154788 (2016).
157. A. G. Mostafa, S. El Attar, F. Mili, E. A. Wright, The effect of environmental temperature on the rate of healing of fractures in tail vertebrae of mice. *J Bone Joint Surg Br* **62-b**, 102-103 (1980).

158. M. A. Flierl *et al.*, Outcomes and complication rates of different bone grafting modalities in long bone fracture nonunions: a retrospective cohort study in 182 patients. *Journal of orthopaedic surgery and research* **8**, 1 (2013).
159. A. R. Amini, C. T. Laurencin, S. P. Nukavarapu, Bone tissue engineering: recent advances and challenges. *Crit Rev Biomed Eng* **40**, 363-408 (2012).
160. A. Jain, S. Kumar, A. N. Aggarwal, N. Jajodia, Augmentation of bone healing in delayed and atrophic nonunion of fractures of long bones by partially decalcified bone allograft (decal bone). *Indian journal of orthopaedics* **49**, 637 (2015).
161. J. L. Marsh, Principles of bone grafting: non-union, delayed union. *Surgery (Oxford)* **24**, 207-210 (2006).
162. T. J. Cypher, J. P. Grossman, Biological principles of bone graft healing. *The Journal of foot and ankle surgery* **35**, 413-417 (1996).
163. T. A. Einhorn, L. C. Gerstenfeld, Fracture healing: mechanisms and interventions. *Nature Reviews Rheumatology* **11**, 45 (2015).
164. M. E. Klontzas *et al.*, Investigational drugs for fracture healing: preclinical & clinical data. *Expert opinion on investigational drugs* **25**, 585-596 (2016).
165. E. A. Barcak, M. J. Beebe, Bone morphogenetic protein: is there still a role in orthopedic trauma in 2017? *The Orthopedic clinics of North America* **48**, 301-309 (2017).
166. M. F. Termaat, F. C. Den Boer, F. C. Bakker, P. Patka, H. J. T. M. Haarman, Bone morphogenetic proteins: development and clinical efficacy in the treatment of fractures and bone defects. *JBJS* **87**, 1367-1378 (2005).
167. S. Boraiah, O. Paul, D. Hawkes, M. Wickham, D. G. Lorich, Complications of recombinant human BMP-2 for treating complex tibial plateau fractures: a preliminary report. *Clinical Orthopaedics and Related Research®* **467**, 3257-3262 (2009).
168. A. W. Ritting, E. W. Weber, M. C. Lee, Exaggerated inflammatory response and bony resorption from BMP-2 use in a pediatric forearm nonunion. *The Journal of hand surgery* **37**, 316-321 (2012).
169. I. Pountos, M. Panteli, T. Georgouli, P. V. Giannoudis, Neoplasia following use of BMPs: is there an increased risk? *Expert opinion on drug safety* **13**, 1525-1534 (2014).
170. G. E. Friedlaender *et al.*, Osteogenic protein-1 (bone morphogenetic protein-7) in the treatment of tibial nonunions: a prospective, randomized clinical trial comparing rhOP-1 with fresh bone autograft. *The Journal of bone and joint surgery. American volume* **83**, S151 (2001).
171. N. K. Kanakaris *et al.*, Application of BMP-7 to tibial non-unions: a 3-year multicenter experience. *Injury* **39**, S83-S90 (2008).
172. S. Govender *et al.*, Recombinant human bone morphogenetic protein-2 for treatment of open tibial fractures: a prospective, controlled, randomized study of four hundred and fifty patients. *JBJS* **84**, 2123-2134 (2002).
173. M. F. Swiontkowski *et al.*, Recombinant human bone morphogenetic protein-2 in open tibial fractures: a subgroup analysis of data combined from two prospective randomized studies. *JBJS* **88**, 1258-1265 (2006).
174. M. Bhandari *et al.*, Study to prospectively evaluate reamed intramedually nails in patients with tibial fractures (SPRINT): study rationale and design. *BMC musculoskeletal disorders* **9**, 91-91 (2008).

175. E. J. Campbell, G. M. Campbell, D. A. Hanley, The effect of parathyroid hormone and teriparatide on fracture healing. *Expert opinion on biological therapy* **15**, 119-129 (2015).
176. Y. Liu *et al.*, Anabolic agents: what is beyond osteoporosis? *Osteoporos Int* **29**, 1009-1022 (2018).
177. P. Aspenberg *et al.*, Teriparatide for acceleration of fracture repair in humans: a prospective, randomized, double-blind study of 102 postmenopausal women with distal radial fractures. *Journal of Bone and Mineral Research* **25**, 404-414 (2010).
178. P. Aspenberg, T. Johansson, Teriparatide improves early callus formation in distal radial fractures: analysis of a subgroup of patients within a randomized trial. *Acta orthopaedica* **81**, 234-236 (2010).
179. P. Peichl, L. A. Holzer, R. Maier, G. Holzer, Parathyroid hormone 1-84 accelerates fracture-healing in pubic bones of elderly osteoporotic women. *JBJS* **93**, 1583-1587 (2011).
180. C. Y. Chiang *et al.*, Teriparatide improves bone quality and healing of atypical femoral fractures associated with bisphosphonate therapy. *Bone* **52**, 360-365 (2013).
181. M. Bhandari *et al.*, Does Teriparatide Improve Femoral Neck Fracture Healing: Results From A Randomized Placebo-controlled Trial. *Clin Orthop Relat Res* **474**, 1234-1244 (2016).
182. T. Johansson, PTH 1-34 (teriparatide) may not improve healing in proximal humerus fractures. A randomized, controlled study of 40 patients.
183. Y. K. Lee, Y. C. Ha, K. H. Koo, Teriparatide, a nonsurgical solution for femoral nonunion? A report of three cases. *Osteoporosis International* **23**, 2897-2900 (2012).
184. L. Xiaofeng, X. Daxia, C. Yunzhen, Teriparatide as a nonoperative treatment for tibial and femoral fracture nonunion: A case report. *Medicine* **96**, (2017).
185. C. Emanuele, P. Leonardo, C. Gianfilippo, A. Matteo, C. Doria, Peri-prosthetic humeral non-union: Where biology meets bio-mechanic. A case report. *International journal of surgery case reports* **39**, 102-105 (2017).
186. D. A. Bednar, Teriparatide treatment of a glucocorticoid-associated resorbing nonunion of a type III odontoid process fracture: a case report. *Clinical Spine Surgery* **26**, E319-E322 (2013).
187. Z. Shi *et al.*, Effectiveness of teriparatide on fracture healing: a systematic review and meta-analysis. *PloS one* **11**, e0168691 (2016).
188. M. Arioka *et al.*, Acceleration of bone regeneration by local application of lithium: Wnt signal-mediated osteoblastogenesis and Wnt signal-independent suppression of osteoclastogenesis. *Biochem Pharmacol* **90**, 397-405 (2014).
189. A. E. Loiselle, S. A. Lloyd, E. M. Paul, G. S. Lewis, H. J. Donahue, Inhibition of GSK-3beta rescues the impairments in bone formation and mechanical properties associated with fracture healing in osteoblast selective connexin 43 deficient mice. *PLoS One* **8**, e81399 (2013).
190. K. L. Lauing, S. Sundaramurthy, R. K. Nauer, J. J. Callaci, Exogenous activation of Wnt/β-Catenin signaling attenuates binge alcohol-induced deficient bone fracture healing. *Alcohol and alcoholism* **49**, 399-408 (2014).

191. K. Vachhani, C. Whyne, Y. Wang, D. M. Burns, D. Nam, Low-dose lithium regimen enhances endochondral fracture healing in osteoporotic rodent bone. *J Orthop Res* **36**, 1783-1789 (2018).
192. Y. Chen *et al.*, Beta-catenin signaling plays a disparate role in different phases of fracture repair: implications for therapy to improve bone healing. *PLoS Med* **4**, e249 (2007).
193. K. Vachhani, A. Pagotto, Y. Wang, C. Whyne, D. Nam, Design of experiments confirms optimization of lithium administration parameters for enhanced fracture healing. *J Biomech* **66**, 153-158 (2018).
194. J. Bernick *et al.*, Parameters for lithium treatment are critical in its enhancement of fracture-healing in rodents. *The Journal of bone and joint surgery. American volume* **96**, 1990 (2014).
195. G. Sisask *et al.*, Rats treated with AZD2858, a GSK3 inhibitor, heal fractures rapidly without endochondral bone formation. *Bone* **54**, 126-132 (2013).
196. M. D. Hoffman, M. Takahata, D. S. M. Benoit. (IEEE), pp. 1-2.
197. S. Lumetti *et al.*, Pharmacological GSK-3beta inhibition improves osteoblast differentiation on titanium surfaces. *J Biol Regul Homeost Agents* **28**, 489-495 (2014).
198. M. D. Hoffman, D. S. W. Benoit, Agonism of Wnt–β-catenin signalling promotes mesenchymal stem cell (MSC) expansion. *Journal of tissue engineering and regenerative medicine* **9**, E13-E26 (2015).
199. W. G. Gunn *et al.*, A crosstalk between myeloma cells and marrow stromal cells stimulates production of DKK1 and interleukin-6: a potential role in the development of lytic bone disease and tumor progression in multiple myeloma. *Stem Cells* **24**, 986-991 (2006).
200. E. Scarpa, University of Southampton, (2016).
201. E. E. Beier *et al.*, Inhibition of beta-catenin signaling by Pb leads to incomplete fracture healing. *J Orthop Res* **32**, 1397-1405 (2014).
202. S. A. Low *et al.*, Healing efficacy of fracture-targeted GSK3beta inhibitor-loaded micelles for improved fracture repair. *Nanomedicine (Lond)* **12**, 185-193 (2017).
203. M. R. Newman, D. S. Benoit, Local and targeted drug delivery for bone regeneration. *Curr Opin Biotechnol* **40**, 125-132 (2016).
204. L. Kyllonen, M. D'Este, M. Alini, D. Eglin, Local drug delivery for enhancing fracture healing in osteoporotic bone. *Acta Biomater* **11**, 412-434 (2015).
205. S. A. Low, C. V. Galliford, J. Yang, P. S. Low, J. i. Kopeček, Biodistribution of fracture-targeted GSK3β inhibitor-loaded micelles for improved fracture healing. *Biomacromolecules* **16**, 3145-3153 (2015).
206. Y. Wang *et al.*, Fracture-Targeted Delivery of beta-Catenin Agonists via Peptide-Functionalized Nanoparticles Augments Fracture Healing. *ACS Nano* **11**, 9445-9458 (2017).
207. E. Scarpa, A. Janeczek, R. O. Oreffo, T. A. Newman, N. D. Evans. (MARY ANN LIEBERT, INC 140 HUGUENOT STREET, 3RD FL, NEW ROCHELLE, NY 10801 USA), vol. 21, pp. S52-S52.
208. P. Lennon, C. Murphy, B. Fennessy, J. P. Hughes, Auditory canal exostoses in Irish surfers. *Irish Journal of Medical Science* **185**, 183-187 (2016).
209. G. E. Kennedy, The relationship between auditory exostoses and cold water: a latitudinal analysis. *Am J Phys Anthropol* **71**, 401-415 (1986).

210. D. F. Harrison, The relationship of osteomata of the external auditory meatus to swimming. *Ann R Coll Surg Engl* **31**, 187-201 (1962).
211. B. Attlmayr, I. M. Smith, Prevalence of 'surfer's ear' in Cornish surfers. *J Laryngol Otol* **129**, 440-444 (2015).
212. M. H. Azizi, Ear disorders in scuba divers. *Int J Occup Environ Med* **2**, 20-26 (2011).
213. W. Hurst, M. Bailey, B. Hurst, Prevalence of external auditory canal exostoses in Australian surfboard riders. *J Laryngol Otol* **118**, 348-351 (2004).
214. J. B. Ramakrishnan, J. A. Pirron, A. Perepletchikov, B. J. Ferguson, Exostoses of the paranasal sinuses. *Laryngoscope* **120**, 2532-2534 (2010).
215. T. Haffey, T. Woodard, R. Sindwani, Paranasal sinus exostoses: an unusual complication of topical drug delivery using cold nasal irrigations. *Laryngoscope* **122**, 1893-1897 (2012).
216. K. M. Schwartz *et al.*, Irrigation nose: CT findings of paranasal sinus exostoses. *Open Neuroimag J* **6**, 90-91 (2012).
217. R. T. Adelson, D. W. Kennedy, Paranasal sinus exostoses: possible correlation with cold temperature nasal irrigation after endoscopic sinus surgery. *Laryngoscope* **123**, 24-27 (2013).
218. V. Alexander, A. Lau, E. Beaumont, A. Hope, The effects of surfing behaviour on the development of external auditory canal exostosis. *Eur Arch Otorhinolaryngol* **272**, 1643-1649 (2015).
219. D. F. Kroon, M. L. Lawson, C. S. Derkay, K. Hoffmann, J. McCook, Surfer's ear: external auditory exostoses are more prevalent in cold water surfers. *Otolaryngol Head Neck Surg* **126**, 499-504 (2002).
220. B. J. Wong *et al.*, Prevalence of external auditory canal exostoses in surfers. *Arch Otolaryngol Head Neck Surg* **125**, 969-972 (1999).
221. H. Nakanishi, T. Tono, H. Kawano, Incidence of external auditory canal exostoses in competitive surfers in Japan. *Otolaryngol Head Neck Surg* **145**, 80-85 (2011).
222. J. E. Fenton, J. Turner, P. A. Fagan, A histopathologic review of temporal bone exostoses and osteomata. *Laryngoscope* **106**, 624-628 (1996).
223. C. E. East, L. Begg, N. E. Henshall, P. R. Marchant, K. Wallace, Local cooling for relieving pain from perineal trauma sustained during childbirth. *Cochrane Database Syst Rev*, Cd006304 (2012).
224. A. L. C. Martimbianco *et al.*, Effectiveness and safety of cryotherapy after arthroscopic anterior cruciate ligament reconstruction. A systematic review of the literature. *YPTSP Physical Therapy in Sport* **15**, 261-268 (2014).
225. C. A. Radkowski *et al.*, Cryotherapy temperature differences after total knee arthroplasty: a prospective randomized trial. *Journal of surgical orthopaedic advances* **16**, 67-72 (2007).
226. C. E. Gibbons, M. C. Solan, D. M. Ricketts, M. Patterson, Cryotherapy compared with Robert Jones bandage after total knee replacement: a prospective randomized trial. *Int Orthop* **25**, 250-252 (2001).
227. T. Gibson, Viability of cartilage after freezing. *Proc R Soc Lond B Biol Sci* **147**, 528-529 (1957).

228. M. A. Serrat, D. King, C. O. Lovejoy, Temperature regulates limb length in homeotherms by directly modulating cartilage growth. *Proceedings of the National Academy of Sciences* **105**, 19348-19353 (2008).
229. C. Gao *et al.*, MSC-seeded dense collagen scaffolds with a bolus dose of VEGF promote healing of large bone defects. *European cells & materials* **26**, 195-207; discussion 207 (2013).
230. J. L. Ramirez-GarciaLuna *et al.*, Defective bone repair in mast cell-deficient Cpa3Cre/+ mice. *PloS one* **12**, e0174396 (2017).
231. D. A. Behrends *et al.*, Defective bone repair in mast cell deficient mice with c-Kit loss of function. *European cells & materials* **28**, 209-221; discussion 221-202 (2014).
232. D. A. Behrends *et al.*, Defective Bone Repair in C57Bl6 Mice With Acute Systemic Inflammation. *Clinical orthopaedics and related research* **475**, 906-916 (2017).
233. A. Hasuike *et al.*, The potency of low-intensity pulsed ultrasound in a rat calvarial guided bone-regeneration model. *J. Hard Tissue Biol. Journal of Hard Tissue Biology* **20**, 217-224 (2011).
234. J. Street *et al.*, Vascular endothelial growth factor stimulates bone repair by promoting angiogenesis and bone turnover. *Proceedings of the National Academy of Sciences of the United States of America* **99**, 9656-9661 (2002).
235. S. Chiba, K. Okada, K. Lee, G. V. Segre, R. M. Neer, Molecular analysis of defect healing in rat diaphyseal bone. *The Journal of veterinary medical science* **63**, 603-608 (2001).
236. H. P. Gerber *et al.*, VEGF couples hypertrophic cartilage remodeling, ossification and angiogenesis during endochondral bone formation. *Nature Medicine* **5**, 623-628 (1999).
237. R. A. Carano, E. H. Filvaroff, Angiogenesis and bone repair. *Drug discovery today* **8**, 980-989 (2003).
238. R. W. K. Wong, A. B. M. Rabie, Early healing pattern of statin-induced osteogenesis. *British Journal of Oral and Maxillofacial Surgery* **43**, 46-50 (2005).
239. A. B. M. Rabie, L. Shum, A. Chayanupatkul, VEGF and bone formation in the glenoid fossa during forward mandibular positioning. *American Journal of Orthodontics and Dentofacial Orthopedics* **122**, 202-209 (2002).
240. G. R. A. Froemming *et al.*, Prolonged effect of moderate and severe hypo-and hyperthermia on Rbm3 and Hsp70 in osteoblast cells. *Bone* **50**, S73-S74 (2012).
241. M. D. Aisha, M. N. Nor-Ashikin, A. B. Sharaniza, The effects of hypo-and hyperthermia on sparc in normal human osteoblast cells. *Regenerative Research* **1**, 62-65 (2012).
242. M. D. Aisha, M. N. Nor-Ashikin, R. Sharanisa, Normal human osteoblast cells exerts an adaptive effect towards moderate hypothermia by retaining bone metabolism and cellular function in vitro. *Bone (Abstracts)* **1**, 193 (2013).
243. M. D. Aisha, M. N. Nor-Ashikin, R. Sharanisa, Moderate hypothermia induces growth arrest in normal human osteoblast cells but retained mitochondrial metabolism in vitro. *Bone (Abstracts)* **1**, 192 (2013).
244. J. Drager, Z. Sheikh, Y. L. Zhang, E. J. Harvey, J. E. Barralet, Local delivery of iron chelators reduces in vivo remodeling of a calcium phosphate bone graft substitute. *Acta biomaterialia* **42**, 411-419 (2016).
245. T. Kiaer, B. Dahl, G. Lausten, Partial pressures of oxygen and carbon dioxide in bone and their correlation with bone-blood flow: effect of decreased arterial supply and venous

congestion on intraosseous oxygen and carbon dioxide in an animal model. *Journal of orthopaedic research : official publication of the Orthopaedic Research Society* **10**, 807-812 (1992).
246. T. Takahashi *et al.*, Ischemia- and cytokine-induced mobilization of bone marrow-derived endothelial progenitor cells for neovascularization. *Nature medicine* **5**, 434-438 (1999).
247. M. T. Engsig *et al.*, Matrix metalloproteinase 9 and vascular endothelial growth factor are essential for osteoclast recruitment into developing long bones. *The Journal of cell biology* **151**, 879-889 (2000).
248. S. Niida *et al.*, Vascular endothelial growth factor can substitute for macrophage colony-stimulating factor in the support of osteoclastic bone resorption. *The Journal of experimental medicine* **190**, 293-298 (1999).
249. M. Nakagawa *et al.*, Vascular endothelial growth factor (VEGF) directly enhances osteoclastic bone resorption and survival of mature osteoclasts. *FEBS</cja:jid> FEBS Letters* **473**, 161-164 (2000).
250. Q. Zhang *et al.*, VEGF-C, a lymphatic growth factor, is a RANKL target gene in osteoclasts that enhances osteoclastic bone resorption through an autocrine mechanism. *The Journal of biological chemistry* **283**, 13491-13499 (2008).
251. Q. Yang *et al.*, VEGF enhancement of osteoclast survival and bone resorption involves VEGF receptor-2 signaling and beta3-integrin. *Matrix biology : journal of the International Society for Matrix Biology* **27**, 589-599 (2008).
252. B. T. MacDonald, K. Tamai, X. He, Wnt/beta-catenin signaling: components, mechanisms, and diseases. *Dev Cell* **17**, 9-26 (2009).
253. N.-G. Kim, C. Xu, B. M. Gumbiner, Identification of targets of the Wnt pathway destruction complex in addition to β-catenin. *Proceedings of the National Academy of Sciences*, pnas-0810185106 (2009).
254. D. Silkstone, H. Hong, B. A. Alman, β-Catenin in the race to fracture repair: in it to Wnt. *Nature Reviews Rheumatology* **4**, 413 (2008).
255. J. B. Regard, Z. Zhong, B. O. Williams, Y. Yang, Wnt signaling in bone development and disease: making stronger bone with Wnts. *Cold Spring Harbor perspectives in biology* **4**, a007997 (2012).
256. F. Takahashi-Yanaga, Activator or inhibitor? GSK-3 as a new drug target. *Biochem Pharmacol* **86**, 191-199 (2013).
257. P. Yin *et al.*, Wnt signaling in human and mouse breast cancer: Focusing on Wnt ligands, receptors and antagonists. *Cancer Sci* **109**, 3368-3375 (2018).
258. B. Taciak, I. Pruszynska, L. Kiraga, M. Bialasek, M. Krol, Wnt signaling pathway in development and cancer. *J Physiol Pharmacol* **69**, (2018).
259. X. Li *et al.*, Wnt signaling in bone metastasis: mechanisms and therapeutic opportunities. *Life Sci* **208**, 33-45 (2018).
260. G. L. Lin, K. D. Hankenson, Integration of BMP, Wnt, and notch signaling pathways in osteoblast differentiation. *J Cell Biochem* **112**, 3491-3501 (2011).
261. D. E. Komatsu *et al.*, Modulation of Wnt signaling influences fracture repair. *Journal of Orthopaedic Research* **28**, 928-936 (2010).

262. D. Castano *et al.*, Noninvasive Localized Cold Therapy: A New Mode of Bone Repair Enhancement. *Tissue Eng Part A*, (2018).
263. S. Iyama *et al.*, A study of the regional distribution of bone formed around hydroxyapatite implants in the tibiae of streptozotocin-induced diabetic rats using multiple fluorescent labeling and confocal laser scanning microscopy. *Journal of periodontology* **68**, 1169-1175 (1997).
264. N. Follak, I. Klöting, E. Wolf, H. Merk, Histomorphometric evaluation of the influence of the diabetic metabolic state on bone defect healing depending on the defect size in spontaneously diabetic BB/OK rats. *Bone* **35**, 144-152 (2004).
265. D. W. Dempster *et al.*, Standardized nomenclature, symbols, and units for bone histomorphometry: a 2012 update of the report of the ASBMR Histomorphometry Nomenclature Committee. *J Bone Miner Res* **28**, 2-17 (2013).
266. Y. Zhang *et al.*, Enhanced osteoclastic resorption and responsiveness to mechanical load in gap junction deficient bone. *PLoS One* **6**, e23516 (2011).
267. J. L. Ramirez-Garcia-Luna *et al.*, Defective bone repair in diclofenac treated C57Bl6 mice with and without lipopolysaccharide induced systemic inflammation. *J Cell Physiol* **234**, 3078-3087 (2019).
268. A. C. Ruifrok, R. L. Katz, D. A. Johnston, Comparison of quantification of histochemical staining by hue-saturation-intensity (HSI) transformation and color-deconvolution. *Appl Immunohistochem Mol Morphol* **11**, 85-91 (2003).
269. A. C. Ruifrok, D. A. Johnston, Quantification of histochemical staining by color deconvolution. *Anal Quant Cytol Histol* **23**, 291-299 (2001).
270. J. Shu, G. E. Dolman, J. Duan, G. Qiu, M. Ilyas, Statistical colour models: an automated digital image analysis method for quantification of histological biomarkers. *Biomedical engineering online* **15**, 46 (2016).
271. M. H. Townsend *et al.*, Non-small-cell lung cancer cell lines A549 and NCI-H460 express hypoxanthine guanine phosphoribosyltransferase on the plasma membrane. *OncoTargets and therapy* **10**, 1921 (2017).
272. Q. G. Shu J, Ilyas M. (2014).
273. J. M. Dominguez *et al.*, Evidence for irreversible inhibition of glycogen synthase kinase-3beta by tideglusib. *J Biol Chem* **287**, 893-904 (2012).
274. A. Heilmann *et al.*, The Wnt serpentine receptor Frizzled-9 regulates new bone formation in fracture healing. *PLoS One* **8**, e84232 (2013).
275. S. L. Dallas, L. F. Bonewald, Dynamics of the transition from osteoblast to osteocyte. *Annals of the New York Academy of Sciences* **1192**, 437-443 (2010).
276. P. Clement-Lacroix *et al.*, Lrp5-independent activation of Wnt signaling by lithium chloride increases bone formation and bone mass in mice. *Proc Natl Acad Sci U S A* **102**, 17406-17411 (2005).
277. Y. Mao *et al.*, Tension force-induced bone formation in orthodontic tooth movement via modulation of the GSK-3β/β-catenin signaling pathway. *Journal of molecular histology* **49**, 75-84 (2018).
278. C. Livingstone, H. Rampes, Lithium: a review of its metabolic adverse effects. *Journal of Psychopharmacology* **20**, 347-355 (2006).

279. T. del Ser *et al.*, Treatment of Alzheimer's disease with the GSK-3 inhibitor tideglusib: a pilot study. *J Alzheimers Dis* **33**, 205-215 (2013).
280. S. Lovestone *et al.*, A phase II trial of tideglusib in Alzheimer's disease. *J Alzheimers Dis* **45**, 75-88 (2015).
281. V. Palomo, A. Martinez, Glycogen synthase kinase 3 (GSK-3) inhibitors: a patent update (2014-2015). *Expert Opin Ther Pat* **27**, 657-666 (2017).
282. C. J. Phiel, P. S. Klein, Molecular targets of lithium action. *Annu Rev Pharmacol Toxicol* **41**, 789-813 (2001).
283. Q. Bao *et al.*, Constitutive beta-catenin activation in osteoblasts impairs terminal osteoblast differentiation and bone quality. *Exp Cell Res* **350**, 123-131 (2017).
284. C. Hartmann, A Wnt canon orchestrating osteoblastogenesis. *Trends Cell Biol* **16**, 151-158 (2006).
285. H. D. Jang, J. Y. Noh, J. H. Shin, J. J. Lin, S. Y. Lee, PTEN regulation by the Akt/GSK-3β axis during RANKL signaling. *Bone* **55**, 126-131 (2013).
286. G. J. Spencer, J. C. Utting, S. L. Etheridge, T. R. Arnett, P. G. Genever, Wnt signalling in osteoblasts regulates expression of the receptor activator of NFκB ligand and inhibits osteoclastogenesis in vitro. *J Cell Sci* **119**, 1283-1296 (2006).
287. V. Krishnan, H. U. Bryant, O. A. Macdougald, Regulation of bone mass by Wnt signaling. *J Clin Invest* **116**, 1202-1209 (2006).
288. J. Albers *et al.*, Canonical Wnt signaling inhibits osteoclastogenesis independent of osteoprotegerin. *J Cell Biol* **200**, 537-549 (2013).